Atmos. Chem. Phys. Discuss., doi:10.5194/acp-2016-1181, 2017
Manuscript under review for journal Atmos. Chem. Phys.
Discussion started: 17 February 2017

Depolarization Ratios Retrieved by AERONET Sun/Sky Radiometer Data and Comparison to Depolarization Ratios Measured With Lidar

Youngmin Noh[1], Detlef Müller[2*], Kyunghwa Lee[3], Kwanchul Kim[3], Kwonho Lee[4]

[1] International Environmental Research Center, Gwangju Institute of Science and Technology (GIST), Korea

[2] University of Hertfordshire, United Kingdom

[3] Gwangju Institute of Science and Technology (GIST), Korea

[4] Gangneung-Wonju National University, Korea

[*]Corresponding Author:

School of Physics, Astronomy and Mathematics, University of Hertfordshire, Hertfordshire, UK

Tel: +44-1707-28-4365

E-mail address: d.mueller@herts.ac.uk (Detlef Müller)

Abstract

The linear particle depolarization ratios at 440, 675, 870, and 1020 nm were derived using data taken with AERONET sun/sky radiometer at Seoul (37.45° N, 126.95° E), Kongju (36.47° N, 127.14° E), Gosan (33.29° N, 126.16° E), and Osaka (34.65° N, 135.59° E). The results are compared to the linear particle depolarization ratio measured by lidar at 532 nm. The correlation coefficient R^2 between the linear particle depolarization ratio derived by AERONET data at 1020 nm and the linear particle depolarization ratio measured with lidar at 532 nm is 0.90, 0.92, 0.79, and 0.89 at Seoul, Kongju, Gosan, and Osaka, respectively. A good correlation between the lidar-measured depolarization ratio at 532 nm and the one retrieved by AERONET at 870 nm. We find correlation coefficients R^2 of 0.89, 0.92, 0.76, and 0.88 at Seoul, Kongju, Gosan, and Osaka, respectively. The correlation coefficient for the data at 675 nm is lower than the correlation coefficient at 870 and 1020 nm. We find correlation values of 0.81, 0.90, 0.64, and 0.81 at Seoul, Kongju, Gosan, and Osaka, respectively. The lowest correlation values are found for the AERONET-derived linear particle depolarization ratio at 440 nm. We find values of 0.38, 0.62, 0.26, and 0.28 at Seoul, Kongju, Gosan, and Osaka, respectively. The linear particle depolarization ratio can be used as a parameter to obtain insight into the variation of optical and microphysical properties of dust when it mixed with anthropogenic pollution particles. The single-scattering albedo decreases with increasing measurement wavelength for low linear particle depolarization ratios. In contrast, single-scattering albedo increases with decreasing wavelength for high linear particle depolarization ratios. The retrieved volume particle size distributions are dominated by the fine-mode fraction if linear particle depolarization ratios are less than 0.15 at 532 nm. The fine-mode fraction of the size distributions decreases and the coarse-mode

Atmos. Chem. Phys. Discuss., doi:10.5194/acp-2016-1181, 2017
Manuscript under review for journal Atmos. Chem. Phys.
Discussion started: 17 February 2017

Atmospheric Chemistry and Physics Discussions
Open Access

fraction of the size distribution increases for increasing the linear particle depolarization ratio at 1020 nm. The dust ratio based on using the linear particle depolarization ratio derived from AERONET data is 0.12 to 0.17 lower than the coarse-mode fraction derived from the volume concentrations of particle size distributions in which case we can compute the coarse-mode fractions of dust.

Key words: linear particle depolarization ratio, lidar, AERONET sun/sky radiometer, dust, single-scattering albedo, size distribution

1. Introduction

There are various aerosol types of natural (primarily desert dust and sea salt) and anthropogenic (primarily combustion of biomass and fossil fuels) origin. A precise understanding of the radiative forcing of these aerosol types is the key to quantifying the aerosol impact on regional and global climate change (IPCC, 2013). In order to better estimate the aerosol effect (direct and indirect radiative forcing) on global climate change many studies have been performed to classify aerosol types (Burton et al., 2013; Eck et al., 2010; 1999; Lee et al., 2010a; Dubovik et al, 2002). However, those studies do not separate aerosol types according to their contribution in a plume of mixed aerosol (respectively mixtures of different aerosol types), but merely classify dominant aerosol types based on the optical properties of aerosols.

Dust is one of the major aerosol components in the global atmosphere. Dust affects Earth's climate by interacting with solar as well as thermal infrared radiation. Dust also affects atmospheric dynamics, atmospheric chemistry, air quality, and ocean biogeochemistry over a wide range of spatial and temporal scales, e.g., Haywood et al. (2005), Jickells et al. (2005) and Husar et al. (2001). On a global average, dust contributes to about one quarter of aerosol optical depth (τ) in the mid-visible wavelength range (Kinne et al., 2006). Dust is also light-absorbing (Lafon et al., 2006 and 2004; Alfaro et al., 2004; Sokolik and Toon, 1999). It is estimated that more than half of aerosol absorption optical depth at 550 nm may come from dust (Chin et al., 2009).

The size distribution and absorption properties of desert dust and other anthropogenic aerosols show properties that can be clearly distinguished (Russel et al., 2010; Dubovik et al., 2002). Desert dust predominately consists of coarse mode particles (typically radius > ~1 μm). In contrast, combustion-produced particles are predominately found in the fine- mode fraction of particle size distributions (typically radius < ~1 μm). Aerosols in which fractions of fine-mode and coarse-mode particles are mixed are among the most challenging aerosol types to characterize. If we can separate desert dust from other aerosols in mixed dust plumes, we improve our understanding of the effect of those mixed aerosol plumes on climate change.

The linear particle depolarization ratio (δ_p) strongly depends on particle shape. Since dust particles have non-spherical shape, the linear particle depolarization ratio can be used to identify the presence of dust particles in the atmosphere. In that regard lidar is a particularly powerful measurement technique (Tesche et al., 2009; Noh et al., 2008; 2007; Iwasaka et al., 2003; Cairo et al., 1999). The δ_p has also been used to identify biogenic aerosols. Noh et al. (2013a,b) and Sassen et al. (2008) identified the vertical distribution of pollen in the atmosphere using the δ_p measured by lidar.The possibility that dust particles are mixed with other, man-made pollution and/or biomass burning particle is very high except in source regions of dust emissions where population density and thus emissions caused by human

Atmos. Chem. Phys. Discuss., doi:10.5194/acp-2016-1181, 2017
Manuscript under review for journal Atmos. Chem. Phys.
Discussion started: 17 February 2017

activities are comparably low (Sun et al., 2010; 2005; Yu et al., 2006). Mixtures of dust particles and anthropogenic particles cause changes in the δ_p of dust plumes. Shin et al. (2015) reported on lidar measurements and show that the δ_p is decreased when dust is mixed with pollution particles. The δ_p is also a very useful parameter that allows us to separate dust from non-dust particles (Anthropogenic, smoke, and sulphate particles) in mixed dust plumes by retrieving the dust ratio (R_D). Shimizu et al. (2004) estimated the contributions of dust and pollution particles in a mixed-dust plume with the assumption that both aerosol types are externally mixed. The optical data of the mixed dust plumes were separated by the R_D into pure dust content and the anthropogenic particles (Noh et al., 2016a; Bravo-Aranda et al., 2015; Noh 2014; Noh et al., 2012b;). Tesche et al. (2011) separated the optical properties of desert dust and biomass burning particles in mixed dust and smoke plumes over the tropical North Atlantic west of the African continent using multi-wavelength aerosol Raman lidar in combination with polarization lidar. Burton et al. (2014) provides a generalized version of the separation methodology between two aerosol types, urban pollution plus dust, marine plus dust, and smoke plus marine by modifying the methodology suggested by Shimizu et al. (2004) and Tesche et al. (2011). Noh (2014) and Tesche et al. (2011; 2009) used the δ_p to retrieve vertically-resolved single-scattering albedo of mixed dust plumes by separating the contribution of dust and non-dust particles. Ansmann et al. (2011) and Navas-Guzmán et al. (2013) separated the contribution of volcanic ash and sulphate particles to total backscatter and extinction coefficient by the δ_p.

Atmos. Chem. Phys. Discuss., doi:10.5194/acp-2016-1181, 2017
Manuscript under review for journal Atmos. Chem. Phys.
Discussion started: 17 February 2017

Atmospheric Chemistry and Physics Discussions
Open Access

However, the numbers of lidar measurement sites are limited and provide only spatially and temporally sparse information on the global scale. Thus we need other methods that could allow us to measure δ_p.

AERONET (Aerosol Robotic NETwork) is an automated, robotic Sun-and-sky-scanning measurement network that currently encompasses more than 797 measurement sites worldwide (http://aeronet.gsfc.nasa.gov/) which span everything from temporally limited observations at sites at which field campaigns were carried out to sites that carry out long-term observations since AERONET started with its observations. AERONET sun/sky radiometers provide globally distributed observations of spectrally-resolved aerosol optical depth (τ) and data inversion products such as particle size distributions and complex refractive indices of different aerosol types (Holben et al., 1998). Dubovik et al. (2006) suggested to use AERONET sun/sky radiometer data to retrieve the δ_p. Müller et al. (2012; 2010) calculated the δ_p of Saharan dust using AERONET sun/sky radiometer data. Noh et al. (2016b) and Lee et al. (2010b) used AERONET sun/sky radiometer data to retrieve the δ_p of Asian dust. However, only cases of nearly pure desert-dust particle were analyzed in these studies. There exist no studies in which the δ_p for various mixtures (mixing ratio) between desert dust and anthropogenic pollution particles using AERONET data has been determined.

In this contribution we are trying to verify the reliability of AERONET-derived δ_p by comparing these values to values of δ_p measured by lidar. Section 2 presents the methods used in this study. Section 3 presents our results. We discuss our results and summarize our findings in section 4.

Atmos. Chem. Phys. Discuss., doi:10.5194/acp-2016-1181, 2017
Manuscript under review for journal Atmos. Chem. Phys.
Discussion started: 17 February 2017

Atmospheric Chemistry and Physics Discussions

2. Methodology

2.1 Study sites

The AERONET sites considered in this study are all located along the pathway of storms (regime of prevailing westerly winds) that serve as major transport routes of Asian dust carried from the arid regions of China and Mongolia. Figure 1 shows the locations of the AERONET sun/sky radiometers and lidar measurement sites used in this study. Seoul (37.45° N, 126.95° E) and Kongju (36.47° N, 127.14° E) are located inland (continental influenced), whereas Gosan (33.29°N, 126.16° E) and Osaka (34.65° N, 135.59° E) are coastal sites. The Gosan site faces the Yellow Sea and is considered an ideal location for monitoring re gional background aerosols in East Asia because there are few local industrial sources in that region. The other three sites are located inside large cities. We also use data from the AERONET site at Dunhuang (40.49° N, 94.95° E) in our study, and we analyzed the depolarization ratios and optical properties of pure Asian dust at this source region.

Lidar data are obtained from the lidar network of the National Institute of Environmental Research (NIES), Japan. The lidars operated in this network are two wavelength (1064 nm, 532nm) Mie-scattering lidars that measure the linear particle depolarization ratio at 532 nm. The details of these lidar systems are explained by Shimizu et al. (2004) and Sugimoto et al. (2008). The locations of the lidar systems used for our research work are the same as the locations of the AERONET systems for the sites in Seoul, Gosan, and Osaka. The lidar used for the Kongju site is located approximately 32 km away from the AERONET site.

2.2 Depolarization ratios derived from data taken with AERONET sun/sky radiometer

Dubovik et al. (2006) introduced kernel look-up tables that describe mixtures of spheroid particles. These kernel look-up tables were used to infer the δ_p of mineral dust observed with Sun/sky radiometer. The details of the AERONET inversion algorithm that processes data of mineral dust are given by Dubovik et al. (2006).

Briefly, the retrieval of the depolarization ratios works as follows. The elements $F_{11}(\lambda)$ and $F_{22}(\lambda)$ of the Müller scattering matrices (Bohren and Huffman, 1983) are computed from the retrieved complex refractive index and particle size distributions. For unpolarized incident light, $F_{11}(\lambda)$ is proportional to the flux of the scattered light (Volten et al., 2001). The $F_{22}(\lambda)$ in turn follows from the angular and spectral distribution of the radiative intensity which is measured with the AERONET instrument (Dubovik et al., 2006). Another input parameter that is needed for the retrieval of the δ_p is the aspect ratio distribution. The aspect ratio indicates the ratio of a particle's longest axis to its shortest axis. In the case of prolate particles its polar diameter is greater than the equatorial diameter, in contrast to oblate particles where this ratio is vice versa. The aspect ratio distribution is kept to a fixed distribution in the AERONET model since scattering elements are nearly equivalent for all mixtures of spheroid particles (Dubovik et al., 2006).

From the ratio of the elements $F_{11}(\lambda)$ and $F_{22}(\lambda)$ at the scattering angle $180°$ the $\delta_p(\lambda)$ can be computed as

Atmos. Chem. Phys. Discuss., doi:10.5194/acp-2016-1181, 2017
Manuscript under review for journal Atmos. Chem. Phys.
Discussion started: 17 February 2017

$$\delta_p(\lambda) = \frac{1 - F_{22}(\lambda, 180°) / F_{11}(\lambda, 180°)}{1 + F_{22}(\lambda, 180°) / F_{11}(\lambda, 180°)} \times 100\ (\%) \qquad (1)$$

The δ_P derived from the sun/sky radiometer data is written as δ_P^S in order to distinguish it from the lidar-derived δ_P (δ_P^L).

The contributions of dust and anthropogenic pollution particles to the total backscatter coefficients of mixed aerosol plumes were estimated from the δ_P under the assumption that both types of aerosol particles are externally mixed. The dust ratio (R_D) of the dust-related backscatter coefficient to the total backscatter coefficient was calculated using Eq. (1), based on the method suggested by Shimizu et al. (2004):

$$R_D = \frac{(\delta_P^S - \delta_2)(1 + \delta_1)}{(\delta_1 - \delta_2)(1 + \delta_P^S)} \qquad (2)$$

where δ_1 and δ_2 denote the δ_P^S of pure dust and non-dust particles (i.e. the total aerosol plume without the contribution by dust), respectively, in the external mixture of aerosol particles. The values δ_1 and δ_2 can be empirically determined. In the present study, we used the value 0.34 for δ_1, which was derived from adding 0.01 to the maximum value observed at the Dunhuang site (Asian dust source region). The value of 0.02 was used for δ_2, which is the minimum value used in this study. When δ_P^S was higher than δ_1 or lower than δ_2, R_D was set to 1 or 0, respectively.

Two kinds of coarse-mode fraction (CMF) were calculated. The coarse-mode fraction of the aerosol optical depth (τ) (CMFτ) is calculated from the ratio of the coarse-mode τ to the total (coarse + fine mode) τ at the same wavelength at which the δ_P^S is available. The coarse-mode fraction is also calculated on the basis of the volume concentration (CMF_{vc}).

Atmos. Chem. Phys. Discuss., doi:10.5194/acp-2016-1181, 2017
Manuscript under review for journal Atmos. Chem. Phys.
Discussion started: 17 February 2017

2.3 Column-integrated depolarization ratio measured by LIDAR

The lidar systems used in our study measure the linear volume depolarization ratio (aerosols + molecules; δ^L) from the linearly and perpendicularly polarized components of the Mie/Rayleigh backscatter signals at 532 nm wavelength (Sakai et al., 2000). The value of δ^L is defined as

$$\delta^L(z) = \frac{P_{\perp}(z)}{P_{||}(z) + P_{\perp}(z)} \times 100\ (\%) = \frac{\beta_{P,\perp}(z) + \beta_{M,\perp}(z)}{\beta_{P,||}(z) + \beta_{M,||}(z) + \beta_{P,\perp}(z) + \beta_{M,\perp}(z)} \times 100\ (\%) \qquad (3)$$

where P(z) is the backscatter signal with respect to height z; β_P and β_M are the volume backscatter coefficients of aerosol particles and air molecules. The symbols $\parallel$ and $\perp$ denote the linearly and perpendicularly polarized components with respect to the plane of polarization of the emitted light, respectively.

The δ_P^L differs from δ^L as it depends on the concentration of particles without taking account of the contribution (concentration) of air molecules. In this contribution, δ_P^L can be calculated according to the definition by Sakai et al. (2000)

$$\delta_P^L(z) = \frac{\beta_{p,\perp}(z)}{\beta_{p,//}(z) + \beta_{p,\perp}(z)} \times 100\ (\%) = \frac{\delta^L(z)R(z) - \delta_M}{R(z) - 1}\ (\%). \qquad (4)$$

The backscatter ratio R is the ratio of the sum of the aerosol backscatter coefficient $(\beta_P + \beta_M)$ to the pure molecular backscatter coefficient (β_M), which, according to Whiteman et al. (1992) can be expressed by

Atmos. Chem. Phys. Discuss., doi:10.5194/acp-2016-1181, 2017
Manuscript under review for journal Atmos. Chem. Phys.
Discussion started: 17 February 2017

$$R(z) = \frac{\beta_P(z) + \beta_M(z)}{\beta_M(z)} \tag{5}$$

The molecular depolarization ratio (δ_M) is assumed to be 0.0044 (Behrendt and Nakamura, 2002).

The parameter δ_P^L can be derived by lidar measurements in terms of vertical profiles. In contrast, δ_P^S describes a column-integrated value. For that reason, δ_P^L had to be changed to column-integrated values in our study, in order to allow for a direct comparison with δ_P^S.

The column integrated weighted δ_P^L (δ_P^{CL}) can be calculated with Eq. (6).

$$\delta_P^{CL} = \int_0^z \delta_P^L(z) W(z) dz \tag{6}$$

where the term W(z) is a weight factor that is calculated on the basis of the measured aerosol backscatter coefficient (β_P) according to the following Eq. (7):

$$W(z) = \frac{\beta_P(z)}{\int_0^z \beta_P(z) dz} \tag{7}$$

Figure 2 shows a retrieval example of δ_P^{CL}. Three cases, corresponding to lidar measurements carried out at 23:00 UTC (start time of measurement) on 13 March 2010 (a), at 06:00 UTC on 22 March 2010 (b), and at 23:15 on 3 May 2010 (c) are shown. The measurement on 13 March 2010 describes an aerosol plume that has a high value of δ_P^L and a high β_P (case 1, Fig. 2 (a)). The measurement on 22 March 2010 describes an aerosol plume with high β_P below and above the planetary boundary layer (PBL), but a high value of δ_P^L is detected only above the PBL (case 2, Fig. 2 (b)). The measurement on 2 May 2010 describes an aerosol plume with low backscatter coefficient and a high value of δ_P^L (case 3, Fig. 2 (c)).

The averaged values of δ_P^L (δ_{ave}) which do not consider the backscatter intensity but just the averaged δ_P^L from bottom to the top height of the profiles of δ_P^L are also listed in Figure 2. The values of δ_P^S at 1020 nm are 0.250, 0.140, and 0.164 for the cases 1, 2, and 3, respectively. The values of δ_P^{CL} are similar to the values of δ_P^S which are 0.243, 0.129, and 0.157 for the cases 1, 2, and 3, respectively. However, the values of δ_{ave} in case 1 and 3 are different compared to δ_P^S. Since δ_P^L is not directly related to aerosol concentration but only to the non-sphericity of (an ensemble of) aerosol particles (in a given volume of air) large values of δ_P^L can occur for high as well as for low aerosol backscatter coefficients. High values of δ_P^L for the situation of high aerosol backscatter coefficients of a thin aerosol layer (Figure 2 (a)) show lower values of δ_{ave} compared to δ_P^S. We find that δ_{ave} are higher than δ_P^S for the situation of a high value δ_P^L in combination with a low aerosol backscatter coefficient (Figure 2 (3)). Those examples in Figure 2 explain that δ_P^{CL} has to be compared with δ_P^S.

3. Results and Discussion

3. 1. Comparison with δ_P^{CL}

Figure 3 shows the temporal variation of τ at 500 nm and the values of δ_P^S at 1020 nm at the four AERONET sites. The combined data of the four sites are shown in the same figure. The number of measurement cases for the four sites are listed in Table 1. The total number of retrieved values of δ_P^S is 163, 44, 139, and 234 at Seoul, Kongju, Gosan, and Osaka, respectively. Since the measurement cases are limited it is hard to analyze seasonal trends. However, we find high values of τ and δ_P^S in spring (March to May). We assume that these high values are caused by transport of dust from East Asia to the Pacific Ocean.

Figure 4 presents scatterplots of δ_P^{CL} and δ_P^S at the four AERONET sites. We compare the values of the δ_P^S at these four wavelengths (440, 675, 870, and 1020 nm) to the δ_P^{CL} at 532 nm. The correlation coefficients R^2 at 1020 nm are high. We find 0.90, 0.92, 0.79, and 0.89 at Seoul, Kongju, Gosan, and Osaka, respectively.

We find similarly high correlation between δ_P^{CL} and δ_P^S at 870 nm, i.e. numbers are 0.89, 0.92, 0.76, and 0.88 at Seoul, Kongju, Gosan, and Osaka, respectively. The correlation at 675 nm is lower compared to the values we find at 870 and 1020 nm. Values are 0.81, 0.90, 0.64, and 0.81 at Seoul, Kongju, Gosan, and Osaka, respectively. The correlation is comparably low at 440 nm. Values are 0.38, 0.62, 0.26, and 0.28 at Seoul, Kongju, Gosan, and Osaka, respectively. The correlation at 440 nm at Kongju is much higher than at the other sites. This higher correlation may be caused by the limited number of observational data and/or observation time. Only 44 cases were taken during a short period of two months, from April to May 2012 at Kongju.

Figure 4 shows that the differences between δ_P^{CL} and δ_P^S are high when the δ_P^{CL} is less than 0.10 at Seoul, Gosan and Osaka. However, the number of cases of low δ_P^{CL} (< 0.10) is comparably low at Kongju compared to the other sites. The number of cases with high δ_P^{CL} (< 0.25) is comparably high (with respect to all cases) compared to what we find for the other sites (see Table 1).

We classified the observational data into 6 groups based on the values of δ_P^S at 1020 nm. Group 1 contains values of less than 0.05 of δ_P^S at 1020 nm. Groups 2, 3, 4, and 5 include

Atmos. Chem. Phys. Discuss., doi:10.5194/acp-2016-1181, 2017
Manuscript under review for journal Atmos. Chem. Phys.
Discussion started: 17 February 2017

Atmospheric Chemistry and Physics
Discussions
Open Access

values between 0.05-0.1, 0.1-0.15, 0.15-0.2, and 0.2-0.25 at 1020 nm, respectively. Values are above 0.25 in group 6.

Table 1 shows the number of data sets (observation cases) for each of the 6 data groups at the four observation sites. The averaged τ at 500 nm, the optical-depth-related Ångström exponent (å) between 440 to 870 nm and the light-absorption-related Ångström exponent ($å_A$, 440 – 870 nm) of each group are also listed in Table 1. The values of τ are similar in all six groups. Reason for that is because τ is insensitive to the shape and size of the particles. The values of $å_A$ increase but values of å decrease with increasing value of δ_P^S.

Figure 5 shows the values δ_P^S of the six groups at the four measurement wavelengths of the AERONET sun/sky radiometers. There is a rather clear increase of δ_P^S with respect to increasing measurement wavelength in group 6. We see a similar pattern in groups 4 and 5, respectively. In contrast, groups 1 - 3 show the highest values of δ_P^S at 440 nm whereas the values of δ_P^S are similar at the other three measurement wavelengths.

Values of δ_P^L of pure mineral dust plumes were measured at three wavelengths (355, 532, and 1064 nm) with lidar (Freudenthaler et al., 2009) during the Saharan Mineral Dust Experiment (SAMUM) in 2006. Freudenthaler et al. (2009) found values of 0.31 of δ_P^L at 532 nm. Müller et al. (2010; 2012) compared those data with data derived from collocated AERONET sun/sky radiometer observations, see Figure 3 in Müller et al. (2010) and Figure 7 in Müller et al. (2012). Values of δ_p from both instruments agree at 1064-nm wavelength. If the sun/sky radiometer results are extrapolated to the lidar wavelength of 355 nm, the δ_p from the sun/sky radiometer is 20 % lower than the value obtained from the lidar observations.

Müller et al. (2010) find that the values of δ_p inferred from the sun/sky radiometer observations tend to be lower than the values measured with lidar for the case of pure mineral dust. Only group 6 (Kongju and Gosan) shows 20% - 30 % lower values of δ_P^S compared to δ_P^{CL} in the visible wavelength range, which is a similar trend reported by Müller et al. (2010). This feature, i.e. that δ_P^{CL} is higher than δ_P^S is also found in group 5. However, the differences of the numbers are less compared to the differences we find for group 6. The values of δ_P^S increase from group 1 to group 6 and the values of δ_P^S are becoming more and more similar to the values of δ_P^{CL} from group 1 to group 6.

Figure 5 shows the δ_P^{CL} at 532 nm of each group. We find 0.27 ± 0.02 and 0.27 ± 0.03 at Kongju and Gosan, respectively, for group 6. The values at the Osaka site are lower. We find 0.21 ± 0.04. The highest values of the δ_P^{CL} is 0.29 at the Kongju and Gosan sites, see Figure 4. The highest value of δ_P^{CL} for the Osaka site is 0.27.

The differences of the δ_p at the observation sites likely are caused by the appearance of dust. The transport distance to the four observation sites may have influence on the values of δ_p. Kongju and Gosan have similar transport distances from the source regions of East Asian dust. Osaka is located in a distance of 1 or 2 days of transport time from Kongju and Gosan. It means that more dust particles can be removed by gravity sedimentation during transport (Maring et al., 2003; Gong et al., 2003). Another reason may be that more anthropogenic pollution particles are mixed into these Asian dust plume because of the longer transport time (Kanayama et al., 2002; Noh et al., 2014; Shin et al., 2015).

Figure 6 shows the averaged values of the vertically resolved β_P, the values of δ_P^L, and the

Atmos. Chem. Phys. Discuss., doi:10.5194/acp-2016-1181, 2017
Manuscript under review for journal Atmos. Chem. Phys.
Discussion started: 17 February 2017

weighted δ_P^L ($\delta_P^L W$) measured by lidar for each group. The backscatter coefficients generally decrease with height. However, high values are found in the upper atmosphere in those cases in which δ_P^L is high. Values of δ_P^L are as high as 0.1 in group 1 and increase with increasing group number (from group 1 to group 6). The increase of the δ_P^L is more obvious above 2-km height than below 2-km height above ground. The higher values above 2-km above ground may be caused by the fact that Asian dust has a relatively lower chance of being mixed with other pollutants if it is transported in the upper parts of the atmosphere (Shin et al., 2015). Especially, group 5 and group 6 show high values of δ_P^L, i.e. larger than 0.3 above 2 km height.

We see that the β_P shows different trends in these two groups. Group 5 has low values of β_P and high values of δ_P^L. In contrast group 6 shows high values of β_P and high values of δ_P^L. This different behavior in these two groups is clearly visible in the values of $\delta_P^L W$. Values of $\delta_P^L W$ in group 5 are less than 2 throughout the whole altitude range. Values of $\delta_P^L W$ are larger than 2 in group 6.

We find that δ_P^S, especially at 1020 nm, is rather similar to δ_P^{CL} and the values of δ_P^S at 1020 nm are large for high dust concentrations and small for low dust concentrations, see Figures 4, 5, and 6. Thus we think that δ_P^S can be a reliable information for identifying the presence of Asian dust particles in East Asian pollution plumes. This means that δ_P^S can be used to retrieve the dust ratio in mixed dust plumes even if vertically-resolved information on the linear particle depolarization ratio is not available.

3. 2. Correlation between δ_{P}^{S} and single-scattering albedo

One main purpose of our study is to estimate the mixing ratio of dust particles with other pollutants in the atmosphere by analyzing δ_{P}^{S}. Another purpose of our study is to estimate on the basis of δ_{P}^{S} the variation of the optical and microphysical properties of dust when it mixes with anthropogenic pollution particles. Correlations between δ_{P}^{S} and other optical parameters allow us to gain insight into these variations.

Variations of aerosol absorption properties can be described by the single-scattering albedo (SSA). The knowledge of the variability of light-absorption of aerosol mixtures discussed in this contribution allows us to assess the direct forcing of mixed-dust plumes. We can also investigate the semi-direct forcing that may occur from atmospheric heating by absorbing aerosol layers (Noh et al., 2012b; 2016b; Noh, 2014). We also investigate how SSA varies with the volume particle size distribution that is corresponding to SSA. For that purpose we use the values of δ_{P}^{S}.

Figure 7 depicts SSA and the volume particle size distribution for each of the 6 groups. The SSA spectra vary with changing δ_{P}^{S} in clearly distinguishable patterns. The SSA spectra of group 1 (low δ_{P}^{S}) show decreasing SSA with increasing wavelength. We find that SSA decreases with increasing measurement wavelength for particle plumes that are dominated by urban-industrial and biomass-burning particles (Dubovik et al., 2002; Giles et al., 2012). Black carbon particles have the strongest light-absorption capacity in the near-infrared wavelength region.

In contrast, the SSA spectra of group 6 (high δ_{P}^{S}) show an increase of SSA with increasing wavelength. The wavelength dependence (i.e. increasing, decreasing, or constant with

Atmos. Chem. Phys. Discuss., doi:10.5194/acp-2016-1181, 2017
Manuscript under review for journal Atmos. Chem. Phys.
Discussion started: 17 February 2017

wavelength) of SSA is an important property that is used in aerosol type classification because the spectral absorption characteristics depend on aerosol type (Giles et al., 2012; Russell et al., 2010; Eck et al., 2010; 2005; Dubovik et al., 2002).

The increase of SSA with increasing wavelength is a characteristic optical feature of desert dust particles (Giles et al., 2012). Dust particles are aggregates of combinations of clay, quartz, and hematite in variable concentration. Dust exhibits strong light-absorption in the UV and at short visible wavelengths (e.g., 440 nm) and lower light-absorption from mid-visible to near infrared wavelengths (Sokolik and Toon, 1999).

Kim et al. (2011) define particles with å < 0.2 as "pure dust" based on observations of dust particles over North Africa and the Arabian Peninsula. The average value of SSA of the "pure dust" part of the aerosol plumes observed at the four observation sites is 0.91, 0.97, 0.97, and 0.97 at 440, 675, 870, and 1020 nm wavelength, respectively.

The SSA spectra of Group 6 at Kongju, Gosan and Osaka resemble the SSA spectra of "pure dust" described by Kim et al. (2011). The SSA of group 6 at Kongju and Gosan show similar values reported by Kim et al. (2011), i.e. 0.94, 0.98, 0.98, and 0.99 at 440, 675, 870, and 1020 nm wavelength, respectively. Lower values of SSA are observed at Osaka. We find 0.88, 0.95, 0.96, and 0.95 at 440, 675, 870, and 1020 nm wavelength, respectively. The differences of SSA at Osaka may be caused by the mixing of pollution particles with dust.

Except for the SSA at 440 nm, the SSA at 675, 870, and 1020 nm show higher values for high δ_p^S at each wavelength. This increase of SSA with increasing δ_p^S results from the mixing of fine-mode pollution particles and coarse-mode Asian dust.

Mixtures of desert dust and pollution aerosols contain two primary particulate light-absorbing species, black carbon in fine-mode particles (Bond and Bergstrom, 2006) and iron oxides in coarse-mode dust particles (Sokolik and Toon, 1999). Iron oxides cause strong light-absorption in the UV and in the short-wavelength range of the visible spectral range of light (Derimian et al., 2008). In pollution particles the principal absorber is soot or black carbon which exhibits light-absorption throughout the entire solar spectrum due to an imaginary part of the complex refractive index that is spectrally relatively constant (Bergstrom et al., 2002). The SSA as a function of δ_P^S shows very little variation at 440 nm compared to the other wavelengths considered in our study (675, 870, and 1020 nm) at the Seoul and Gosan sites. Eck et al. (2010) suggest that this kind of restricted SSA-values at 440 nm is induced when both, coarse-mode-aerosol dominated mixtures (desert dust) and fine-mode-dominated aerosol mixtures (pollution) have relatively similar magnitudes of light-absorption with regard to the light-scattering at that wavelength.

The lower (440 nm) and similar SSAs (675, 870, and 1020 nm) in group 6 compared to the SSAs in group 5 are shown for the Osaka site. High concentrations of fine-mode particles with strong light-absorbing property can cause a decreasing SSA at the four wavelengths 440, 675, 870, and 1020 nm.

The variations of the fine-mode and the coarse-mode part of the size distributions are clearly shown in Figure 7. Group 1 contains fine-mode dominated particle size distributions. The fine-mode part of the particle size distributions decreases and the coarse-mode part of the size distributions increases for increasing δ_P^S. The variations of Cv_c/Cv_f for each group in Table 2 show these tendencies more clearly.

The values of Cv_c/Cv_f increase as we move from group 1 to 6. The values of Cv_c/Cv_f in group 1 are similar at Seoul, Kongju, Gosan, and Osaka. We find 0.29, 0.32, 0.35, and 0.28, respectively. The values of Cv_c/Cv_f are similar for all three observation sites in each of the

Atmos. Chem. Phys. Discuss., doi:10.5194/acp-2016-1181, 2017
Manuscript under review for journal Atmos. Chem. Phys.
Discussion started: 17 February 2017

groups 1 - 5.

However, in the case of group 6, Cvc/Cvf is 7.6, 11.3, and 8.6 at Kongju, Gosan, and Osaka, respectively. The values of Cv_c/Cv_f in group 6 are smaller than the average value at Dunhuang. The average value of Cv_c/Cv_f at Dunhuang is 15.0 ± 2.6, see Table 4. Cv_c/Cv_f decreases if fine-mode pollution particles are mixed into a dust plume and/or if coarse-mode dust particles are removed from the plume during long-range transport.

3. 3. δ_P^S, SSA, and particle size distribution at the dust source region

We analyzed the AERONET sun/sky radiometer data taken in the source region of Asian dust and evaluated the optical properties and δ_P^S of "pure Asian dust". Figure 8 shows δ_P^S, SSA and volume particle size distributions observed on 5 days in one of the source regions of Asian dust, i.e. Dunhuang in 2012. Values of δ_P^S at 440 nm are characteristic of pure dust particles, i.e. we find values larger than 0.25. SSA increases with increasing measurement wavelength which is also characteristic of pure dust. We find this behavior on all days except for the data representing 8 April 2012. We find that the SSA at each wavelength (at the Dunhuang site) is higher than the SSA retrieved at the corresponding wavelengths for sites in North Africa and the Arabian Peninsula (Kim et al., 2011; Müller et al., 2010).

Table 3 lists τ, δ_P^S at 1020 nm, and å, $å_A$, CMF_{vc} and R_D. The values of å observed at Dunhuang on all measurement dates used in this study are such that they can be considered as representing pure dust, as suggested by Kim et al. (2011). The exception is the measurement on 8 April. On that day we find δ_P^S = 0.25 at 1020 nm and $å_A$ = 1.76, which are comparably lower values than the values retrieved for the other observation days. In addition, volume particle size distributions retrieved for 8 April (see Figure 8) show a higher peak modal volume radius for the coarse-mode size distribution compared to what is typically found for size distributions of desert dust (Dubovik et al. 2002; Müller et al., 2010; 2012). We conclude that particles observed on 8 April describe a mixed-dust plume rather than a pure dust plume.

We compare the average values of δ_P^S, SSA, and the volume particle size distributions observed at Dunhuang with the respective values of group 6 at Kongju, Gosan, and Osaka. We exclude the data taken on 8 April at Dunhuang for the calculation of the average values because that data likely do not represent pure Asian dust. Figure 9 shows our comparison results.

The highest values of δ_P^S at Dunhuang are 0.26, 0.28, 0.30, and 0.33 at 440, 675, 870, and 1020 nm wavelength, respectively. The spectral behavior of δ_P^S (at the four wavelengths) at Kongju, Gosan, and Osaka is similar to the spectral behavior of δ_P^S retrieved for the Dunhuang site. However, the values of δ_P^S at the four measurement wavelengths at Kongju, Gosan, and Osaka are 0.04 - 0.05 lower than the respective values at the Dunhuang site. This difference between Dunhuang and the other three sites may be caused by gravitational settling of coarse mode dust particles during transport and/or a higher share of anthropogenic pollution particles that may enter the dust plume during long-range transport from the source region to the other three sites.

The volume particle size distributions shown in Figure 9 (c) corroborate our assumption. The volume concentration of the coarse mode particles is as low as 0.36, 0.44, and 0.33 ($\mu m^3/\mu m^2$) in the far-field sites of Kongju, Gosan, and Osaka, respectively. We find that among all days during which we observed pure Asian dust at Dunhuang, the minimum value of 0.49 ($\mu m^3/\mu m^2$) was found on 9 April 2012, see Figure 9 (c) and Table 4.

Figure 9 (b) shows a comparison of the spectral SSA between Dunhuang and the other three

Atmos. Chem. Phys. Discuss., doi:10.5194/acp-2016-1181, 2017
Manuscript under review for journal Atmos. Chem. Phys.
Discussion started: 17 February 2017

sites. The average values of SSA at Dunhuang are 0.94, 0.98, 0.98, and 0.98 at 440, 675, 870, and 1020 nm, respectively. The value of 0.94 for SSA at 440 nm at the Dunhuang site is higher than the SSA of "pure dust" observed over North Africa and the Arabian Peninsula (Kim et al., 2011; Müller et al., 2011; Müller et al., 2010).

As noticed previously, iron oxides cause the strongest light-absorption in the ultraviolet and at visible wavelengths (Derimian et al., 2008). We assume that the differences of SSA at 440 nm between the Dunhuang site and observation sites in North Africa and the Arabian Peninsula are caused by differences of the chemical composition of dust particles, as for example the concentration of iron oxides in the dust particles at these different sites.

Our results show that nearly-pure dust may be transported to Kongju and Gosan from long distances, and that the coarse mode fraction of the particle size distribution may not necessarily increase in that case. The spectral behavior of SSA and its values at each wavelength at the Kongju and Gosan sites which are long-range transport sites match with the values of SSA at Dunhuang. This match suggests that there may be a similar chemical composition of the dust, and perhaps similar concentrations of iron oxide in the dust observed at Dunhuang, Kongju, and Gosan.

SSA values at Osaka are lower than those at Kongju and Gosan. We find values of 0.88, 0.95, 0.96, and 0.95 at 440, 675, 870, and 1020 nm, respectively. These low SSAs can be caused by the mixing of pollution particles. We first investigate the vertical distribution of the dust plumes of group 6 at Osaka. The vertical distribution of particles in the dust plumes of group 6 at Osaka can be clearly distinguished according to their observation date.

Figure 10 shows the separated values of β_P, δ_P^L, and δ_P^L W (dust and non-dust contribution) in terms of case 1 and 2 for group 6 at Osaka according to the observation date. The data

Atmos. Chem. Phys. Discuss., doi:10.5194/acp-2016-1181, 2017
Manuscript under review for journal Atmos. Chem. Phys.
Discussion started: 17 February 2017

Atmospheric Chemistry and Physics Discussions

taken on 14 and 15 March 2010 (case 1) show that the dust plumes are distributed up to 3.5 km height above ground. The main part of the dust plumes is located between 1 and 2 km height on both days. The values of δ_P^L are above 0.25 in that height range. The β_P-values of the dust plume are lower below 1 km height compared to what we find for β above 1 km above ground. The value of δ_P^L varies between 0.1 and 0.12 and thus is lower compared to what we find between 1 and 2 km height.

The dust plumes extend to 2 km height above ground on 2 May 2011 (measurement case 2). We find high values of β_P near the surface. Values of 0.3 – 0.4 for δ_P^L are higher than depolarization ratios found for case 1.

Case 1 is quite different from case 2 if we look at δ_P^LW. The values of δ_P^LW of case 1 are mainly affected by Asian dust that is present above 1 km height above ground. Values for case 2 are mainly influenced by Asian dust near the surface.

These differences of the height above ground of the main portions of the dust plumes may be one reason why the light-absorption capacity of the two cases differs. There is a higher possibility that pollutants can be mixed during long-range transport in case 2.

Figure 11 corroborates our assumption. Figure 11 shows values of δ_P^S, SSA, and volume particle size distributions for two cases. The values of δ_P^S and SSA in case 1 show a similar values compared to the case of pure dust observed at Dunhuang. Values of these parameters are different from those at Dunhuang for case 2. Particularly, the values of SSA of case 2 are significantly lower than SSA-values at Dunhuang. Moreover, SSAs at 1020 nm are lower than those at 870 nm for case 2. This difference of absolute values and the differences of the spectral behavior may be caused by the mixing of dust with light-absorbing pollutants, such

Atmos. Chem. Phys. Discuss., doi:10.5194/acp-2016-1181, 2017
Manuscript under review for journal Atmos. Chem. Phys.
Discussion started: 17 February 2017

as black carbon, when we take account of the vertical distribution of the dust plume; see Figure 10.

The differences of $å_A$ between case 1 and case 2 (Table 5) support this observation. $å_A$ in case 1 is 2.12 which points to pure dust. In contrast, $å_A$ in case 2 is 1.58 which is more likely representative of a mixture of dust with pollutants (Russell et al., 2010).

Figure 12 shows backward trajectories. The transport pattern is different for case 1 and case 2. The main portions of the dust plumes of case 1 passed over source regions of major pollution emissions in China and Korea at heights above 1.5 – 2 km, i.e., above the planetary boundary layer, before the plumes arrived over Osaka. Since most of the pollution resides in the PBL the possibility is low that the main dust layer mixed with pollutants. In contrast to case 1, case 2 indicates that pollutants were mixed into the Asian dust layers while they were transported near the surface and within the PBL over industrialized areas and before they arrived over Osaka. Shin et al. (2015) reported that more pollution particles can be mixed into dust plumes if these plumes are transported at low altitude above ground.

Table 5 shows that Cv_c/Cv_f for case 2 is 11.8 which is higher than the value of 6.8 for case 1. The increase of the fine-mode particle concentration may not be the only reason that can cause this decrease. Other reasons that may contribute to a decrease of Cv_c/Cv_f are for example the coating of coarse-mode dust particles by absorbing fine-mode pollution particles. There is considerable evidence of the coating of dust particles by absorbing fine-mode pollution particles in the East Asian region. Respective observations were made during the ACE-Asia campaign in spring 2001 (Huebert et al., 2003; Kim et al., 2004). Arimoto et al. (2006) also present scanning electron microscopy images showing black carbon particles adhering onto the surface of coarse-mode dust, with typically 15% - 30% of the dust surface

Atmos. Chem. Phys. Discuss., doi:10.5194/acp-2016-1181, 2017
Manuscript under review for journal Atmos. Chem. Phys.
Discussion started: 17 February 2017

coated by black carbon, which likely increases the absorption.

3. 4. Retrieval of Dust ratio using sun/sky radiometer derived Depolarization ratio

The concept of separating lidar backscatter signals caused by the contribution of dust particles in mixed dust plumes to the total backscatter signals using δ_p has already been applied to lidar measurements (Shimizu et al., 2004; Noh, 2014; Tesche et al., 2009). With regard to AERONET sun/sky radiometer data R_D is calculated from Eq. (2) (see section 2) and the use of δ_p^S at 1020 nm.

The retrieved R_D is compared with CMF_{vc}. The comparison between R_D retrieved from AERONET data and CMF_{vc} allows us to distinguish between non-dust coarse-mode particles and dust.

Figure 13 shows the correlation between R_D and CMF_{vc} in terms of R^2. We find a comparably high correlation between R_D and CMF_{vc}. Values are 0.72, 0.95, 0.77, and 0.93 at Seoul, Kongju, Gosan, and Osaka, respectively.

R_D describes the ratio of dust particles to other types of non-spherical aerosols in the atmosphere. Unlike R_D, CMF_{vc} considers the size of particles and is uncorrelated to the shape of the particles. Since most of the dust particles belong to the coarse-mode fraction, the value of CMF_{vc} increases alongside with the dust ratio. However, the coarse-mode of a particle size distribution does not include dust only but also contains large particles that are generated by physical and chemical reactions, e.g. coagulation, condensation processes, and hygroscopic growth.

Figure 13 shows that CMF_{vc} is on average 0.12-0.17 higher than R_D at the four observation

Atmos. Chem. Phys. Discuss., doi:10.5194/acp-2016-1181, 2017
Manuscript under review for journal Atmos. Chem. Phys.
Discussion started: 17 February 2017

Atmospheric Chemistry and Physics
Discussions

sites, which implies that non-dust particles are present, i.e., even though dust particles for the most part belong to the coarse-mode fraction of particle size distributions, not all coarse-mode particles are dust particles. The average values of CMF_{vc} and the differences between R_D and CMF_{vc} for each of the 6 groups are listed in Table 1.

R_D of groups 1 – 5 is 0.11 - 0.19 lower than CMF_{vc} at the four sites. The differences between R_D and CMF_{vc} are lower for group 6. We find 0.4, 0.4, and 0.3 at Kongju, Gosan, and Osaka, respectively.

We find a similar difference for the Dunhuang site, see Table 3. The average values of R_D and CMF_{vc} are 0.97 ± 0.02 and 0.94 ± 0.01, respectively, except for the case of 8 April. This means that most of the coarse-mode particles are composed of dust particles. However, pollution and/or biomass burning particles can be injected into the dust plume during transport from the source region. These particles may contribute to the coarse mode of the volume particle size distribution. If the dust plume is transported at low altitude above ground, there is an increased possibility that dust mixes with other aerosols (Shin et al., 2015).

This increased possibility is corroborated by the results for the case of Osaka in group 6. Table 5 shows for this case that δ_P^S, SSA, and the particle size distribution clearly depend on the altitude of the dust plume. R_D and CMF_{vc} show very similar values with respect to case 1. The average value of the difference between R_D and CMF_{vc} is 0.004 ± 0.008 for the case that the main part of the dust plume is transported above the planetary boundary layer (case 1). This difference between R_D and CMF_{vc} increases to 0.11 ± 0.04 when the dust plume is transported near the surface, as can be seen from δ_P^L W of case 2. From these results we can confirm that the coarse mode is mostly composed of pure dust particles without that mixing with other types of particle has occurred during transport above the PBL. However, the ratio

Atmos. Chem. Phys. Discuss., doi:10.5194/acp-2016-1181, 2017
Manuscript under review for journal Atmos. Chem. Phys.
Discussion started: 17 February 2017

of dust particles to non-dust coarse-mode particles decreases as the result of mixing processes during transport. These phenomena can be explained by the variation of the volume median radius (Rv).

The volume median radius of the coarse mode (Rv_c) of 3.21-3.27 μm for urban-industrial aerosols generated by fossil fuel combustion and biomass burning aerosol produced by forest and grassland fires is higher than Rv_c of 2.62-3.05 μm of desert dust (Dubovik et al., 2002; Eck et al., 2010). The average Rv_c decreases as δ_P^S increases. In this study, Rv_c shows low values when the observed particles are nearly pure dust. The average Rv_c at Dunhuang is 1.88 μm (except 8 April 2012). This value is quite similar to 2 μm of Rv_c for dust that originated from China and was measured over Japan (Tanaka et al., 1989). The average Rv_c at Osaka decreases from 2.85 to 2.46 to 2.20 to 1.94 to 2.08 to 1.85 μm between group 1 and group 6, respectively. The other sites show the same pattern of decreasing values between groups 1 to 6. The average Rv_c of 2.15 at Kongju and 1.77 μm at Gosan (group 6) also shows similar values to the values found in the dust source region. The average Rv_c of the other groups is higher than Rv_c of dust in the source region. We find the highest values in group 1, i.e. 3.05, 2.72, 2.58, and 2.85 μm at Seoul, Kongju, Gosan, and Osaka, respectively.

4. Summary and Conclusion

In this study we attempt to verify the reliability of the AERONET sun/sky radiometer derived linear particle depolarization ratio (δ_P^S) that can be used for detecting dust particles by comparing this parameter to the linear particle depolarization ratios measured by lidar (δ_P^L). We considered low (cases dominated by pollution particles) to high linear particle depolarization ratios (cases dominated by Asian dust) at four downwind regions (Seoul,

Atmos. Chem. Phys. Discuss., doi:10.5194/acp-2016-1181, 2017
Manuscript under review for journal Atmos. Chem. Phys.
Discussion started: 17 February 2017

Kongju, Gosan and Osaka) of Asian dust. We calculated the column-integrated weighted δ_P^L (δ_P^{CL}) and compared these values with δ_P^S. The strongest correlation exists between δ_P^S at 1020 nm and δ_P^{CL}. Values are 0.90, 0.92, 0.79, and 0.89 for the sites at Seoul, Kongju, Gosan, and Osaka, respectively. A good correlation was also observed at 870 nm. We find values of 0.89, 0.92, 0.76, and 0.88 at Seoul, Kongju, Gosan, and Osaka, respectively. Although the correlation at 675 nm is weaker than the one at 870 and 1020 nm, we still find a comparably high correlation of 0.81, 0.90, 0.64, and 0.81 at Seoul, Kongju, Gosan, and Osaka, respectively. The correlation coefficient at 440 nm is comparably low. We find values of 0.38, 0.62, 0.26, and 0.28 at Seoul, Kongju, Gosan, and Osaka, respectively.

We are of the opinion that δ_P^S can be used as a parameter to estimate the variation of optical and microphysical properties of dust when it is mixed with anthropogenic pollution particles. There is a clear pattern of variation of the fine and coarse modes of the volume particle size distributions with regard to changes of the value of δ_P^S. Fine-mode dominant volume particle size distributions are present for low values of δ_P^S. The fine-mode fraction of the volume particle size distribution decreases and the coarse-mode fraction of the particle size distribution increases when the δ_P^S at 1020 nm increases.

The SSA spectra show clearly distinguishable patterns according to the variation of δ_P^S at 1020 nm. The SSA decreases with increasing measurement wavelength for low values of δ_P^S. In contrast, the SSA increases with decreasing wavelength for high values of δ_P^S.

The dust ratio (R_D) can be derived from the δ_P^S. The R_D is approximately 0.12 to 0.17 lower than what we find from the coarse-mode fraction of the volume concentration (CMF_{vc}).

However, if δ_P^S is larger than 0.25, then R_D is similar to CMF_{vc}, and the difference between these two parameters is less than 0.04. We conclude that the δ_P^S at 1020 nm can be used to estimate the dust ratio. The dust ratio estimated in that way can then be used to calculate the mass concentration of Asian dust and air pollutants as column-integrated value.

We can confirm that δ_P^S, especially at 1020 nm, is in good agreement with δ_P^{CL} and provides comparably reliable information that allows us to distinguish the presence of Asian dust particles in mixed aerosol plumes. The consistency indicates that the values of δ_P^S at 1020 nm are high for high dust concentrations and small for low dust concentrations. This means that δ_P^S can be used to retrieve the dust ratio in mixed dust plumes. However, we need to keep in mind that we cannot identify the vertical distribution of dust particles on the basis of δ_P^S because δ_P^S is a column-integrated value.

Acknowledgement

This work was funded by the Korea Meteorological Administration Research and Development Program under Grant KMIPA 2015-6150. This work was supported by a National Research Foundation of Korea (NRF) grant funded by the Korean government (MEST) (NRF-2015R1D1A1A09058269). This research was also supported by the International Environmental Research Center (IERC).

References

Alfaro, S. C., Lafon, S., Rajot, J. L., Formenti, P., Gaudichet, A. and Maillé, M.: Iron oxides and light absorption by pure desert dust: An experimental study, J. Geophys. Res., 109(D8), D08208, doi:10.1029/2003JD004374, 2004.

Ansmann, A., et al.: Ash and fine-mode particle mass profiles from EARLINET-AERONET observations over central Europe after the eruptions of the Eyjafjallajökull volcano in 2010, J. Geophys. Res., 116, D00U02,doi:10.1029/2010JD015567., 2011.

Arimoto, R., Kim, Y. J., Kim, Y. P., Quinn, P. K., Bates, T. S., Anderson, T. L., Gong, S., Uno, I., Chin, M., Huebert, B. J., Clarke, A. D., Shinozuka, Y., Weber, R. J., Anderson, J. R., Guazzotti, S. A., Sullivan, R. C., Sodeman, D. A., Prather, K. A. and Sokolik, I. N.: Characterization of Asian Dust during ACE-Asia, Global and Planetary Change, 52(1–4), 23–56, doi:10.1016/j.gloplacha.2006.02.013, 2006.

Behrendt, A. and Nakamura, T.: Calculation of the calibration constant of polarization lidar and its dependency on atmospheric temperature, Opt. Express, OE, 10(16), 805–817, doi:10.1364/OE.10.000805, 2002.

Bergstrom, R. W., Russell, P. B., and Hignett, P.: Wavelength dependence of the absorption of black carbon particles: Predictions and results from the TARFOX experiment and implications for the aerosol single scattering albedo, J. Atmos. Sci., 59, 567–577, 2002.

Bohren, C. F. and Huffman, D. R.: Absorption and Scattering by a Sphere, in Absorption and Scattering of Light by Small Particles, pp. 82–129, Wiley-VCH Verlag GmbH. [online] Available from: http://onlinelibrary.wiley.com/doi/10.1002/9783527618156.ch4/summary (Accessed 27 December 2016), 1983.

Bond, T. C. and Bergstrom, R. W.: Light Absorption by Carbonaceous Particles: An Investigative Review, Aerosol Science and Technology, 40(1), 27–67, doi:10.1080/02786820500421521, 2006.

Bravo-Aranda, J. A., Titos, G., Granados-Munoz, M. J., GuerreroRascado, J. L., Navas-Guzman, F., Valenzuela, A., Lyamani, H., Olmo, F. J., Andrey, J., and Alados-Arboledas, L.: Study of mineral dust entrainment in the planetary boundary layer by lidar depolarisation technique, Tellus B, 67, 26180, doi:10.3402/tellusb.v67.26180, 2015.

Burton, S. P., Ferrare, R. A., Vaughan, M. A., Omar, A. H., Rogers, R. R., Hostetler, C. A. and Hair, J. W.: Aerosol classification from airborne HSRL and comparisons with the CALIPSO vertical feature mask, Atmos. Meas. Tech., 6(5), 1397–1412, doi:10.5194/amt-6-1397-2013, 2013.

Burton, S.P., Vaughan, M.A., Ferrare, R.A., Hostetler, C.A.: Separating mixtures of aerosol types in airborne High Spectral Resolution Lidar data. Atmos. Meas. Tech. 7, 419-436. 2014.

Cairo, F., Donfrancesco, G. D., Adriani, A., Pulvirenti, L. and Fierli, F.: Comparison of various linear depolarization parameters measured by lidar, Appl. Opt., AO, 38(21), 4425–4432, doi:10.1364/AO.38.004425, 1999.

Chin, M., Diehl, T., Dubovik, O., Eck, T. F., Holben, B. N., Sinyuk, A. and Streets, D. G.: Light absorption by pollution, dust, and biomass burning aerosols: a global model study and evaluation with AERONET measurements, Ann. Geophys., 27(9), 3439–3464, doi:10.5194/angeo-27-3439-2009, 2009.

Atmos. Chem. Phys. Discuss., doi:10.5194/acp-2016-1181, 2017
Manuscript under review for journal Atmos. Chem. Phys.
Discussion started: 17 February 2017

Derimian, Y., Karnieli, A., Kaufman, Y. J., Andreae, M. O., Andreae, T. W., Dubovik, O., Maenhaut, W. and Koren, I.: The role of iron and black carbon in aerosol light absorption, Atmos. Chem. Phys., 8(13), 3623–3637, doi:10.5194/acp-8-3623-2008, 2008.

Dubovik, O., Holben, B., Eck, T. F., Smirnov, A., Kaufman, Y. J., King, M. D., Tanré, D. and Slutsker, I.: Variability of Absorption and Optical Properties of Key Aerosol Types Observed in Worldwide Locations, J. Atmos. Sci., 59(3), 590–608, doi:10.1175/1520-0469(2002)059<0590:VOAAOP>2.0.CO;2, 2002.

Dubovik, O., Sinyuk, A., Lapyonok, T., Holben, B. N., Mishchenko, M., Yang, P., Eck, T. F., Volten, H., Muñoz, O., Veihelmann, B., van der Zande, W. J., Leon, J.-F., Sorokin, M. and Slutsker, I.: Application of spheroid models to account for aerosol particle nonsphericity in remote sensing of desert dust, J. Geophys. Res., 111(D11), D11208, doi:10.1029/2005JD006619, 2006.

Eck, T. F., Holben, B. N., Reid, J. S., Dubovik, O., Smirnov, A., O'Neill, N. T., Slutsker, I. and Kinne, S.: Wavelength dependence of the optical depth of biomass burning, urban, and desert dust aerosols, J. Geophys. Res., 104(D24), 31333–31349, doi:10.1029/1999JD900923, 1999.

Eck, T. F., Holben, B. N., Dubovik, O., Smirnov, A., Goloub, P., Chen, H. B., Chatenet, B., Gomes, L., Zhang, X.-Y., Tsay, S.-C., Ji, Q., Giles, D. and Slutsker, I.: Columnar aerosol optical properties at AERONET sites in central eastern Asia and aerosol transport to the tropical mid-Pacific, J. Geophys. Res., 110(D6), D06202, doi:10.1029/2004JD005274, 2005.

Eck, T. F., Holben, B. N., Sinyuk, A., Pinker, R. T., Goloub, P., Chen, H., Chatenet, B., Li, Z., Singh, R. P., Tripathi, S. N., Reid, J. S., Giles, D. M., Dubovik, O., O'Neill, N. T., Smirnov, A., Wang, P. and Xia, X.: Climatological aspects of the optical properties of fine/coarse mode aerosol mixtures, J. Geophys. Res., 115(D19), D19205, doi:10.1029/2010JD014002, 2010.

Freudenthaler, V., Esselborn, M., Wiegner, M., Heese, B., Tesche, M., Ansmann, A., Müller, D., Althausen, D., Wirth, M., Fix, A., Ehret, G., Knippertz, P., Toledano, C., Gasteiger, J., Garhammer, M. and Seefeldner, M.: Depolarization ratio profiling at several wavelengths in pure Saharan dust during SAMUM 2006, Tellus B, 61(1), 165–179, doi:10.1111/j.1600-0889.2008.00396.x, 2009.

Giles, D. M., Holben, B. N., Eck, T. F., Sinyuk, A., Smirnov, A., Slutsker, I., Dickerson, R. R., Thompson, A. M. and Schafer, J. S.: An analysis of AERONET aerosol absorption properties and classifications representative of aerosol source regions, J. Geophys. Res., 117(D17), D17203, doi:10.1029/2012JD018127, 2012.

Gong, S. L., Zhang, X. Y., Zhao, T. L., McKendry, I. G., Jaffe, D. A. and Lu, N. M.: Characterization of soil dust aerosol in China and its transport and distribution during 2001 ACE-Asia: 2. Model simulation and validation, J. Geophys. Res., 108(D9), 4262, doi:10.1029/2002JD002633, 2003.

Atmos. Chem. Phys. Discuss., doi:10.5194/acp-2016-1181, 2017
Manuscript under review for journal Atmos. Chem. Phys.
Discussion started: 17 February 2017

Haywood, J. M., Allan, R. P., Culverwell, I., Slingo, T., Milton, S., Edwards, J. and Clerbaux, N.: Can desert dust explain the outgoing longwave radiation anomaly over the Sahara during July 2003?, J. Geophys. Res., 110(D5), D05105, doi:10.1029/2004JD005232, 2005.

Holben, B. N., Eck, T. F., Slutsker, I., Tanré, D., Buis, J. P., Setzer, A., Vermote, E., Reagan, J. A., Kaufman, Y. J., Nakajima, T., Lavenu, F., Jankowiak, I. and Smirnov, A.: AERONET—A Federated Instrument Network and Data Archive for Aerosol Characterization, Remote Sensing of Environment, 66(1), 1–16, doi:10.1016/S0034-4257(98)00031-5, 1998.

Huebert, B. J., Bates, T., Russell, P. B., Shi, G., Kim, Y. J., Kawamura, K., Carmichael, G. and Nakajima, T.: An overview of ACE-Asia: Strategies for quantifying the relationships between Asian aerosols and their climatic impacts, J. Geophys. Res., 108(D23), 8633, doi:10.1029/2003JD003550, 2003.

Husar, R. B., Tratt, D. M., Schichtel, B. A., Falke, S. R., Li, F., Jaffe, D., Gassó, S., Gill, T., Laulainen, N. S., Lu, F., Reheis, M. C., Chun, Y., Westphal, D., Holben, B. N., Gueymard, C., McKendry, I., Kuring, N., Feldman, G. C., McClain, C., Frouin, R. J., Merrill, J., DuBois, D., Vignola, F., Murayama, T., Nickovic, S., Wilson, W. E., Sassen, K., Sugimoto, N. and Malm, W. C.: Asian dust events of April 1998, J. Geophys. Res., 106(D16), 18317–18330, doi:10.1029/2000JD900788, 2001.

IPCC: Climate Change 2013 - The Physical Science Basis: Working Group I Contribution to the Fifth Assessment Report of the Intergovernmental Panel on Climate Change [Stocker, T.F., D. Qin, G.-K. Plattner, M. Tignor, S.K. Allen, J. Boschung, A. Nauels, Y. Xia, V. Bex and P.M. Midgley (eds.)], Cambridge University Press Cambridge, UK, and New York, NY, USA., 2013.

Iwasaka, Y., Shibata, T., Nagatani, T., Shi, G.-Y., Kim, Y. S., Matsuki, A., Trochkine, D., Zhang, D., Yamada, M., Nagatani, M., Nakata, H., Shen, Z., Li, G., Chen, B. and Kawahira, K.: Large depolarization ratio of free tropospheric aerosols over the Taklamakan Desert revealed by lidar measurements: Possible diffusion and transport of dust particles, J. Geophys. Res., 108(D23), 8652, doi:10.1029/2002JD003267, 2003.

Jickells, T. D., An, Z. S., Andersen, K. K., Baker, A. R., Bergametti, G., Brooks, N., Cao, J. J., Boyd, P. W., Duce, R. A., Hunter, K. A., Kawahata, H., Kubilay, N., laRoche, J., Liss, P. S., Mahowald, N., Prospero, J. M., Ridgwell, A. J., Tegen, I. and Torres, R.: Global Iron Connections Between Desert Dust, Ocean Biogeochemistry, and Climate, Science, 308(5718), 67–71, doi:10.1126/science.1105959, 2005.

Kanayama, S., Yabuki, S., Yanagisawa, F. and Motoyama, R.: The chemical and strontium isotope composition of atmospheric aerosols over Japan: the contribution of long-range-transported Asian dust (Kosa), Atmospheric Environment, 36(33), 5159–5175, doi:10.1016/S1352-2310(02)00587-3, 2002.

Kim, D., Chin, M., Yu, H., Eck, T. F., Sinyuk, A., Smirnov, A. and Holben, B. N.: Dust optical properties over North Africa and Arabian Peninsula derived from the AERONET dataset, Atmos. Chem. Phys., 11(20), 10733–10741, doi:10.5194/acp-11-10733-2011, 2011.

Kim, K. W., He, Z. and Kim, Y. J.: Physicochemical characteristics and radiative properties of Asian dust particles observed at Kwangju, Korea, during the 2001 ACE-Asia intensive observation period, J. Geophys. Res., 109(D19), D19S02, doi:10.1029/2003JD003693, 2004.

Kinne, S., Schulz, M., Textor, C., Guibert, S., Balkanski, Y., Bauer, S. E., Berntsen, T., Berglen, T. F., Boucher, O., Chin, M., Collins, W., Dentener, F., Diehl, T., Easter, R., Feichter, J., Fillmore, D., Ghan, S., Ginoux, P., Gong, S., Grini, A., Hendricks, J., Herzog, M., Horowitz, L., Isaksen, I., Iversen, T., Kirkevåg, A., Kloster, S., Koch, D., Kristjansson, J. E., Krol, M., Lauer, A., Lamarque, J. F., Lesins, G., Liu, X., Lohmann, U., Montanaro, V., Myhre, G., Penner, J., Pitari, G., Reddy, S., Seland, O., Stier, P., Takemura, T. and Tie, X.: An AeroCom initial assessment – optical properties in aerosol component modules of global models, Atmos. Chem. Phys., 6(7), 1815–1834, doi:10.5194/acp-6-1815-2006, 2006.

Lafon, S., Rajot, J.-L., Alfaro, S. C. and Gaudichet, A.: Quantification of iron oxides in desert aerosol, Atmospheric Environment, 38(8), 1211–1218, doi:10.1016/j.atmosenv.2003.11.006, 2004.

Lafon, S., Sokolik, I. N., Rajot, J. L., Caquineau, S. and Gaudichet, A.: Characterization of iron oxides in mineral dust aerosols: Implications for light absorption, J. Geophys. Res., 111(D21), D21207, doi:10.1029/2005JD007016, 2006.

Lee, J., Kim, J., Song, C. H., Ryu, J.-H., Ahn, Y.-H. and Song, C. K.: Algorithm for retrieval of aerosol optical properties over the ocean from the Geostationary Ocean Color Imager, Remote Sensing of Environment, 114(5), 1077–1088, doi:10.1016/j.rse.2009.12.021, 2010a.

Lee, K.-H., Muller, D., Noh, Y.-M., Shin, S.-K. and Shin, D.-H.: Depolarization Ratio Retrievals Using AERONET Sun Photometer Data, J. Opt. Soc. Korea, JOSK, 14(3), 178–184, 2010b.

Maring, H., Savoie, D. L., Izaguirre, M. A., Custals, L. and Reid, J. S.: Mineral dust aerosol size distribution change during atmospheric transport, J. Geophys. Res., 108(D19), 8592, doi:10.1029/2002JD002536, 2003.

Mikami, M., Shi, G. Y., Uno, I., Yabuki, S., Iwasaka, Y., Yasui, M., Aoki, T., Tanaka, T. Y., Kurosaki, Y., Masuda, K., Uchiyama, A., Matsuki, A., Sakai, T., Takemi, T., Nakawo, M., Seino, N., Ishizuka, M., Satake, S., Fujita, K., Hara, Y., Kai, K., Kanayama, S., Hayashi, M., Du, M., Kanai, Y., Yamada, Y., Zhang, X. Y., Shen, Z., Zhou, H., Abe, O., Nagai, T., Tsutsumi, Y., Chiba, M. and Suzuki, J.: Aeolian dust experiment on climate impact: An overview of Japan–China joint project ADEC, Global and Planetary Change, 52(1–4), 142–172, doi:10.1016/j.gloplacha.2006.03.001, 2006.

Müller, D., Ansmann, A., Freudenthaler, V., Kandler, K., Toledano, C., Hiebsch, A., Gasteiger, J., Esselborn, M., Tesche, M., Heese, B., Althausen, D., Weinzierl, B., Petzold, A. and von Hoyningen-Huene, W.: Mineral dust observed with AERONET Sun photometer,

Atmos. Chem. Phys. Discuss., doi:10.5194/acp-2016-1181, 2017
Manuscript under review for journal Atmos. Chem. Phys.
Discussion started: 17 February 2017

Raman lidar, and in situ instruments during SAMUM 2006: Shape-dependent particle properties, J. Geophys. Res., 115(D11), D11207, doi:10.1029/2009JD012523, 2010.

Müller, D., Lee, K.-H., Gasteiger, J., Tesche, M., Weinzierl, B., Kandler, K., Müller, T., Toledano, C., Otto, S., Althausen, D. and Ansmann, A.: Comparison of optical and microphysical properties of pure Saharan mineral dust observed with AERONET Sun photometer, Raman lidar, and in situ instruments during SAMUM 2006, J. Geophys. Res., 117(D7), D07211, doi:10.1029/2011JD016825, 2012.

Müller, T., Schladitz, A., Kandler, K. and Wiedensohler, A.: Spectral particle absorption coefficients, single scattering albedos and imaginary parts of refractive indices from ground based in situ measurements at Cape Verde Island during SAMUM-2, Tellus B, 63(4), doi:10.3402/tellusb.v63i4.16348, 2011.

Navas-Guzma´avas-Guzmadoi:1ller, J. A. Bravo-Aranda, J. L. Guerrero-Rascado, M. J. Granados-Mun˜uoz, D. PeDrez-Ramı´rez, F. J. Olmo, and L. Alados-Arboledas,: Eruption of the Eyjafjallajo¨ykull Volcano in spring 2010: Multiwavelength Raman lidar measurements of sulphate particles in the lower troposphere, J. Geophys. Res. Atmos., 118, 1804–1813, doi:10.1002/jgrd.50116, 2013.

Noh, Y. M.: Single-scattering albedo profiling of mixed Asian dust plumes with multiwavelength Raman lidar, Atmospheric Environment, 95, 305–317, doi:10.1016/j.atmosenv.2014.06.028, 2014.

Noh, Y. M., Kim, Y. J., Choi, B. C. and Murayama, T.: Aerosol lidar ratio characteristics measured by a multi-wavelength Raman lidar system at Anmyeon Island, Korea, Atmospheric Research, 86(1), 76–87, doi:10.1016/j.atmosres.2007.03.006, 2007.

Noh, Y. M., Kim, Y. J. and Müller, D.: Seasonal characteristics of lidar ratios measured with a Raman lidar at Gwangju, Korea in spring and autumn, Atmospheric Environment, 42(9), 2208–2224, doi:10.1016/j.atmosenv.2007.11.045, 2008.

Noh, Y. M., Müller, D., Lee, H., Lee, K. and Kim, Y. J.: Columnar aerosol optical and radiative properties according to season and air mass transport pattern over East Asia, Environ Monit Assess, 184(8), 4763–4775, doi:10.1007/s10661-011-2300-7, 2012a.

Noh, Y. M., Müller, D., Lee, H., Lee, K., Kim, K., Shin, S. and Kim, Y. J.: Estimation of radiative forcing by the dust and non-dust content in mixed East Asian pollution plumes on the basis of depolarization ratios measured with lidar, Atmospheric Environment, 61, 221–231, doi:10.1016/j.atmosenv.2012.07.034, 2012b.

Noh, Y. M., Müller, D., Lee, H. and Choi, T. J.: Influence of biogenic pollen on optical properties of atmospheric aerosols observed by lidar over Gwangju, South Korea, Atmospheric Environment, 69, 139–147, doi:10.1016/j.atmosenv.2012.12.018, 2013a.

Noh, Y. M., Lee, H., Mueller, D., Lee, K., Shin, D., Shin, S., Choi, T. J., Choi, Y. J. and Kim, K. R.: Investigation of the diurnal pattern of the vertical distribution of pollen in the lower

Atmos. Chem. Phys. Discuss., doi:10.5194/acp-2016-1181, 2017
Manuscript under review for journal Atmos. Chem. Phys.
Discussion started: 17 February 2017

Atmospheric Chemistry and Physics
Open Access
Discussions

troposphere using LIDAR, Atmos. Chem. Phys., 13(15), 7619–7629, doi:10.5194/acp-13-7619-2013, 2013b.

Noh, Y. M., Shin, S.-K., Lee, K., Müller, D. and Kim, K.: Utilization of the depolarization ratio derived by AERONET Sun/sky radiometer data for type confirmation of a mixed aerosol plume over East Asia, International Journal of Remote Sensing, 37(10), 2180–2197, doi:10.1080/01431161.2016.1176274, 2016a.

Noh, Y. M., Lee, K., Kim, K., Shin, S.-K., Müller, D. and Shin, D. H.: Influence of the vertical absorption profile of mixed Asian dust plumes on aerosol direct radiative forcing over East Asia, Atmospheric Environment, 138, 191–204, doi:10.1016/j.atmosenv.2016.04.044, 2016b.

Russell, P. B., Bergstrom, R. W., Shinozuka, Y., Clarke, A. D., DeCarlo, P. F., Jimenez, J. L., Livingston, J. M., Redemann, J., Dubovik, O. and Strawa, A.: Absorption Angstrom Exponent in AERONET and related data as an indicator of aerosol composition, Atmos. Chem. Phys., 10(3), 1155–1169, doi:10.5194/acp-10-1155-2010, 2010.

Sakai, T., Nagai, T., Nakazato, M., Mano, Y. and Matsumura, T.: Ice clouds and Asian dust studied with lidar measurements of particle extinction-to-backscatter ratio, particle depolarization, and water-vapor mixing ratio over Tsukuba, Appl Opt, 42(36), 7103–7116, 2003.

Sassen, K., Wang, Z. and Liu, D.: Global distribution of cirrus clouds from CloudSat/Cloud-Aerosol Lidar and Infrared Pathfinder Satellite Observations (CALIPSO) measurements, J. Geophys. Res., 113(D8), D00A12, doi:10.1029/2008JD009972, 2008.

Shimizu, A., Sugimoto, N., Matsui, I., Arao, K., Uno, I., Murayama, T., Kagawa, N., Aoki, K., Uchiyama, A. and Yamazaki, A.: Continuous observations of Asian dust and other aerosols by polarization lidars in China and Japan during ACE-Asia, J. Geophys. Res., 109(D19), D19S17, doi:10.1029/2002JD003253, 2004.

Shin, S.-K., Müller, D., Lee, C., Lee, K. H., Shin, D., Kim, Y. J. and Noh, Y. M.: Vertical variation of optical properties of mixed Asian dust/pollution plumes according to pathway of air mass transport over East Asia, Atmos. Chem. Phys., 15(12), 6707–6720, doi:10.5194/acp-15-6707-2015, 2015.

Sokolik, I. N. and Toon, O. B.: Incorporation of mineralogical composition into models of the radiative properties of mineral aerosol from UV to IR wavelengths, J. Geophys. Res., 104(D8), 9423–9444, doi:10.1029/1998JD200048, 1999.

Sugimoto, N., Matsui, I., Shimizu, A., Nishizawa, T., Hara, Y., Xie, C., Uno, I., Yumimoto, K., Wang, Z. and Yoon, S.-C.: Lidar network observations of tropospheric aerosols, vol. 7153, p. 71530A–71530A–13., 2008.

Sun, Y., Zhuang, G., Wang, Y., Zhao, X., Li, J., Wang, Z. and An, Z.: Chemical composition of dust storms in Beijing and implications for the mixing of mineral aerosol with pollution

Atmos. Chem. Phys. Discuss., doi:10.5194/acp-2016-1181, 2017
Manuscript under review for journal Atmos. Chem. Phys.
Discussion started: 17 February 2017

aerosol on the pathway, J. Geophys. Res., 110(D24), D24209, doi:10.1029/2005JD006054, 2005.

Sun, Y., Zhuang, G., Huang, K., Li, J., Wang, Q., Wang, Y., Lin, Y., Fu, J. S., Zhang, W., Tang, A. and Zhao, X.: Asian dust over northern China and its impact on the downstream aerosol chemistry in 2004, J. Geophys. Res., 115(D7), D00K09, doi:10.1029/2009JD012757, 2010.

Tanaka, M., Nakajima, T., Shiobara, M., Yamano, M., and Arao, K.: Aerosol optical characteristics in the yellow sand events observed in May, 1982 at Nagasaki—Part 1. Observations. J. Meteor. Soc. Japan, 67, 267–278, 1989.

Tesche, M., Ansmann, A., Müller, D., Althausen, D., Engelmann, R., Freudenthaler, V. and Groß, S.: Vertically resolved separation of dust and smoke over Cape Verde using multiwavelength Raman and polarization lidars during Saharan Mineral Dust Experiment 2008, J. Geophys. Res., 114(D13), D13202, doi:10.1029/2009JD011862, 2009.

Tesche, M., Müller, D., Gross, S., Ansmann, A., Althausen, D., Freudenthaler, V., Weinzierl, B., Veira, A. and Petzold, A.: Optical and microphysical properties of smoke over Cape Verde inferred from multiwavelength lidar measurements, Tellus B, 63(4), 677–694, doi:10.1111/j.1600-0889.2011.00549.x, 2011.

Volten, H., Muñoz, O., Rol, E., de Haan, J. F., Vassen, W., Hovenier, J. W., Muinonen, K. and Nousiainen, T.: Scattering matrices of mineral aerosol particles at 441.6 nm and 632.8 nm, J. Geophys. Res., 106(D15), 17375–17401, doi:10.1029/2001JD900068, 2001.

Whiteman, D. N., Melfi, S. H. and Ferrare, R. A.: Raman lidar system for the measurement of water vapor and aerosols in the Earth's atmosphere, Appl Opt, 31(16), 3068–3082, 1992.

Yu, X., Cheng, T., Chen, J. and Liu, Y.: A comparison of dust properties between China continent and Korea, Japan in East Asia, Atmospheric Environment, 40(30), 5787–5797, doi:10.1016/j.atmosenv.2006.05.013, 2006.

Figure captions

Figure 1. Map of the observation sites. Measurements with AERONET sun/sky radiometer and lidar were performed at Seoul, Kongju, Gosan, and Osaka. AERONET sun/sky radiometer measurements were made at Dunhuang.

Atmos. Chem. Phys. Discuss., doi:10.5194/acp-2016-1181, 2017
Manuscript under review for journal Atmos. Chem. Phys.
Discussion started: 17 February 2017

Figure 2. Lidar derived aerosol backscatter coefficient (β_P; black line), the linear particle depolarization ratio (δ_P^L ; green), and the weighted linear particle depolarization ratio (δ_P^L W; gray) at 532 nm observed (a) from 23:00 – 23:15 UTC on 13 March 2010, (b) from 06:00 – 06:15 UTC on 22 March 2010, and (c) from 23:15 - 23:30 on 3 May 2010. The wavelength of δ_P^S is 1020 nm. The height is expressed as a.g.l.

Figure 3. Aerosol optical depth (τ) measured with sun/sky radiometer at 500 nm (black squares) and linear particle depolarization ratio derived at 1020 nm from sun/sky radiometer data (δ_P^S ; blue open circles). (a) data of the four sites taken from 2010 to 2014, (b) data taken at Seoul for two years (2012 and 2013), (c) data taken at Kongju in spring 2012, and (d) data taken at Gosan during four years (2011 – 2014), mostly during spring, and (e) data taken from 2010 – 2014 at Osaka.

Figure 4. The correlation coefficients R^2 (the coefficient of determination) between δ_P^{CL} at 532 and δ_P^S at 440 (black squares), 675 (red circles), 870 (blue open triangles), and 1020 nm (orange diamonds) at (a) Seoul, (b) Kongju, (c) Gosan, and (d) Osaka.

Figure 5. The average value of the δ_P^S at 440, 675, 870, and 1020 nm for each group. Each group is distinguished by color: black (group 1), red (group 2), blue (group 3), pink (group 4), gray (group 5), and orange (group 6). The average values of the δ_P^{CL} at 532 nm are shown as open circles and the same color as the δ_P^S.

Atmos. Chem. Phys. Discuss., doi:10.5194/acp-2016-1181, 2017
Manuscript under review for journal Atmos. Chem. Phys.
Discussion started: 17 February 2017

Atmospheric Chemistry and Physics
Discussions
Open Access

Figure 6. Average values of the vertical profiles of (1) the particle backscatter coefficient, (2) the linear particle depolarization ratios (δ_p^L), and (3) the weighted linear particle depolarization ratios (δ_p^L w) for group 1 (a), group 2 (b), group 3 (c), group 4 (d), group 5 (e), and group 6 (f). The sites are Seoul (red), Kongju (orange), Gosan (blue), and Osaka (black).

Figure 7. Average value of the SSA and the volume particle size distributions of each of the 6 groups considered in this study: group 1 (black), group 2 (red), group 3 (blue), group 4 (pink) , group 5 (gray), and group 6 (orange).

Figure 8. (a) Linear particle depolarization ratios, (b) single-scattering albedos, and (c) volume particle size distributions derived from sun/sky radiometer observations at Dunhuang.

Figure 9. Comparison between (a) δ_p^S, (b) SSA, and volume particle size distributions representing the dust source region (Dunhuang, black) and group-6-data (Kongju, blue), (Gosan, gray), and (Osaka, red).

Figure 10. Separation of data of group 6 at Osaka according to case 1 (black) and case 2 (red). Shown are (a) backscatter coefficients, (b) linear particle depolarization ratios (δ_p^L), and (c) weighted linear particle depolarization ratios (δ_p^L W).

Atmos. Chem. Phys. Discuss., doi:10.5194/acp-2016-1181, 2017
Manuscript under review for journal Atmos. Chem. Phys.
Discussion started: 17 February 2017

Figure 11. The (a) δ_P^S at 440, 675, 870, and 1020 nm, (b) SSA at 440, 675, 870, and 1020 nm, and (c) volume particle size distributions. Shown are the results for case 1 (black) and case 2 (red). Cv_c/Cv_f is inserted in (c). The observation site is Osaka.

Figure 12. HYSPLIT 5-days backward trajectories of dust plumes for case 1 (a) and case (2). The start height for case 1 is 1200 m (blue), 1500 m (red), and 1800 m (yellow). For case 2 it is 500 m (blue), 1000 m (red), and 1500 m (yellow). The start time is 0:00 UTC in each case.

Figure 13. Correlation plots of the dust ratio at 1020 nm versus the volume concentration in the coarse-mode fraction.

Atmos. Chem. Phys. Discuss., doi:10.5194/acp-2016-1181, 2017
Manuscript under review for journal Atmos. Chem. Phys.
Discussion started: 17 February 2017

Atmospheric Chemistry and Physics
Open Access
EGU
Discussions

Table 1. Average value of aerosol optical depth (τ) at 500 nm, optical-depth-related Ångström exponent (å, 440 – 870 nm), absorption-related Ångström exponent ($å_A$), dust ratio (R_D) derived by δ_p^S at 1020 nm, coarse-mode fraction of the τ at 1020 nm, coarse-mode fraction of the volume concentration (CMF_{vc}), and difference between CMF_{vc} and R_D.

DPR (1020)		Group 1	Group 2	Group 3	Group 4	Group 5	Group 6	Total
		0 - 0.05	0.05 - 0.1	0.1 - 0.15	0.15 - 0.2	0.2 - 0.25	0.25 >	
Seoul	#	25	74	38	21	5		163
	τ (500 nm)	0.62 ± 0.26	0.74 ± 0.31	0.77 ± 0.29	0.62 ± 0.25	0.89 ± 0.29		0.72 ± 0.29
	å	1.42 ± 0.21	1.38 ± 0.16	1.22 ± 0.16	1.05 ± 0.12	0.8 ± 0.15		1.29 ± 0.22
	$å_A$	1.32 ± 0.37	1.56 ± 0.43	1.78 ± 0.40	1.8 ± 0.29	1.88 ± 0.36		1.62 ± 0.43
	R_D	0.08 ± 0.04	0.22 ± 0.05	0.37 ± 0.05	0.51 ± 0.05	0.63 ± 0.05		0.29 ± 0.15
	CMFτ[1]	0.13 ± 0.06	0.29 ± 0.14	0.46 ± 0.12	0.69 ± 0.06	0.78 ± 0.02		0.37 ± 0.21
	CMF_{vc}	0.22 ± 0.06	0.38 ± 0.11	0.56 ± 0.09	0.70 ± 0.05	0.79 ± 0.06		0.45 ± 0.18
	$CMF_{vc} - R_D$	0.14	0.16	0.19	0.19	0.16		0.16
Kongju	#	1	22	8	3		10	44
	τ (500 nm)	0.67	0.68 ± 0.29	0.69 ± 0.24	0.41 ± 0.01		0.61 ± 0.21	0.65 ± 0.25
	å	1.74	1.55 ± 0.12	1.27 ± 0.16	1.09 ± 0.07		0.4 ± 0.10	1.21 ± 0.47
	$å_A$	1.25	1.32 ± 0.21	1.54 ± 0.47	1.43 ± 0.72		2.28 ± 0.29	1.58 ± 0.50
	R_D	0.08	0.21 ± 0.04	0.40 ± 0.06	0.54 ± 0.03		0.85 ± 0.06	0.41 ± 0.26
	CMFτ[1]	0.23	0.29 ± 0.09	0.47 ± 0.16	0.66 ± 0.03		0.90 ± 0.02	0.49 ± 0.26
	CMF_{vc}	0.24	0.36 ± 0.07	0.54 ± 0.11	0.65 ± 0.01		0.88 ± 0.02	0.53 ± 0.22
	$CMF_{vc} - R_D$	0.16	0.15	0.14	0.11		0.04	0.12
Gosan	#	18	47	47	19	5	3	139
	τ (500 nm)	0.6 ± 0.24	0.54 ± 0.23	0.54 ± 0.17	0.53 ± 0.14	0.41 ± 0.02	0.85 ± 0.17	0.55 ± 0.20
	å	1.55 ± 0.14	1.34 ± 0.20	1.27 ± 0.18	0.92 ± 0.18	0.77 ± 0.11	0.24 ± 0.24	0.124 ± 0.30
	$å_A$	0.75 ± 0.36	0.91 ± 0.48	0.94 ± 0.43	0.95 ± 0.59	1.01 ± 0.11	2.39 ± 0.70	0.94 ± 0.51
	R_D	0.08 ± 0.02	0.20 ± 0.05	0.37 ± 0.04	0.53 ± 0.04	0.71 ± 0.02	0.85 ± 0.05	0.32 ± 0.18
	CMFτ[1]	0.24 ±0.07	0.33 ± 0.15	0.53 ± 0.11	0.69 ± 0.10	0.81 ± 0.02	0.90 ± 0.02	0.47 ± 0.21
	CMF_{vc}	0.26 ± 0.06	0.37 ± 0.10	0.56 ± 0.09	0.68 ± 0.08	0.75 ± 0.05	0.89 ± 0.08	0.49 ± 0.18
	$CMF_{vc} - R_D$	0.18	0.17	0.19	0.15	0.04	0.04	0.17
Osaka	#	54	80	32	38	20	10	234
	τ (500 nm)	0.54 ± 0.21	0.47 ± 0.18	0.47 ± 0.12	0.54 ± 0.15	0.61 ± 0.17	0.58 ± 0.15	0.51 ± 0.18
	å	1.64 ± 0.13	1.52 ± 0.16	0.13 ± 0.17	1.01 ± 0.14	0.70 ± 0.18	0.26 ± 0.08	1.31 ± 0.39
	$å_A$	1.18 ± 0.25	1.23 ± 0.23	1.37 ± 0.43	1.69 ± 0.39	1.57 ± 0.43	1.98 ± 0.41	1.37 ± 0.39
	R_D	0.07 ± 0.04	0.20 ± 0.06	0.37 ± 0.06	0.55 ± 0.05	0.68 ± 0.04	0.86 ± 0.04	0.32 ± 0.23
	CMFτ[1]	0.17 ± 0.09	0.30 ± 0.12	0.47 ± 0.14	0.69 ± 0.07	0.81 ± 0.04	0.91 ± 0.01	0.43 ± 0.26
	CMF_{vc}	0.21 ± 0.06	0.35 ± 0.07	0.52 ± 0.08	0.66 ± 0.05	0.79 ± 0.06	0.89 ± 0.03	0.45 ± 0.22
	$CMF_{vc} - R_D$	0.14	0.15	0.15	0.11	0.11	0.03	0.13

[1] 1020 nm

Table 2. Averaged volume concentration of the fine (Cv_f) and the coarse mode (Cv_c), and the ratio (Cv_c/Cv_f) for the 6 groups.

		Group 1	Group 2	Group 3	Group 4	Group 5	Group 6	Total
		0 - 0.05	0.05 - 0.1	0.1 - 0.15	0.15 - 0.2	0.2 - 0.25	0.25 >	
Seoul	Cv_f	0.112 ± 0.051	0.117 ± 0.052	0.103 ± 0.042	0.067 ± 0.032	0.082 ± 0.021		0.11 ± 0.05
	Cv_c	0.031 ± 0.013	0.069 ± 0.032	0.132 ± 0.052	0.162 ± 0.071	0.352 ± 0.172		0.098 ± 0.081
	Cv_c/Cv_f	0.29 ± 0.10	0.66 ± 0.29	1.39 ± 0.54	2.45 ± 0.65	4.26 ± 1.60		1.11 ± 0.99
Kongju	Cv_f	0.136	0.109 ± 0.044	0.092 ± 0.038	0.046 ± 0.004		0.048 ± 0.018	0.088 ± 0.044
	Cv_c	0.044	0.062 ± 0.027	0.105 ± 0.029	0.085 ± 0.012		0.361 ± 0.148	0.138 ± 0..140
	Cv_c/Cv_f	0.32	0.59 ± 0.19	1.29 ± 0.63	1.84 ± 0.12		7.61 ± 1.44	2.37 ± 2.95
Gosan	Cv_f	0.127 ± 0.043	0.104 ± 0.044	0.081 ± 0.036	0.074 ± 0.038	0.042 ± 0.002	0.054 ± 0.039	0.091 ± 0.043
	Cv_c	0.043 ± 0.016	0.059 ± 0.027	0.105 ± 0.042	0.159 ± 0.068	0.136 ± 0.059	0.444 ± 0.125	0.098 ± 0.077
	Cv_c/Cv_f	0.35 ± 0.12	0.63 ± 0.31	1.40 ± 0.57	2.36 ± 0.89	3.18 ± 1.21	11.26 ± 7.07	1.41 ± 1.92
Osaka	Cv_f	0.103 ± 0.037	0.077 ± 0.030	0.065 ± 0.019	0.066 ± 0.018	0.059 ± 0.016	0.039 ± 0.008	0.076 ± 0.031
	Cv_c	0.027 ± 0.011	0.040 ± 0.015	0.072 ± 0.028	0.135 ± 0.047	0.253 ± 0.147	0.326 ± 0.094	0.087 ± 0.097
	Cv_c/Cv_f	0.28 ± 0.11	0.56 ± 0.18	1.13 ± 0.35	2.04 ± 0.43	4.49 ± 2.58	8.49 ± 2.55	1.49 ± 2.10

Table 3. Aerosol optical depth (τ) at 500 nm, linear particle depolarization ratio (δ_p^S) derived from the sun/sky radiometer data, optical-depth-related Ångström exponent (å, 440-870 nm), absorption-related Ångström exponent ($å_A$), coarse-mode fraction in terms of the volume concentration (CMF_{vc}), and dust ratio (R_D) at 1020 nm. The observation site is Dunhuang.

Date	τ (500 nm)	δ_p^S (1020 nm)	å (440-870 nm)	$å_A$	CMF_{vc}	R_D
8 Apr.	0.71	0.25	0.13	1.76	0.94	0.77
9 Apr.	0.92	0.31	0.12	2.17	0.93	0.94
26 Apr.	1.17	0.32	0.14	2.14	0.94	0.96
27 Apr.	1.00	0.34	0.15	2.46	0.95	0.99
28 Apr.	1.16	0.32	0.17	2.19	0.93	0.96
Ave.[1]	0.97 ± 0.17	0.31 ± 0.03	0.14 ± 0.02	2.14 ± 0.25	0.94 ± 0.01	0.93 ± 0.09
Ave.[2]	1.04 ± 0.11	0.33 ± 0.01	0.14 ± 0.02	2.24 ± 0.15	0.94 ± 0.01	0.97 ± 0.02

[1]Averaged for all data [2]Averaged except 8 Apr. data

Atmos. Chem. Phys. Discuss., doi:10.5194/acp-2016-1181, 2017
Manuscript under review for journal Atmos. Chem. Phys.
Discussion started: 17 February 2017

Atmospheric Chemistry and Physics
Discussions
Open Access

Table 4. Volume concentration of the fine (Cv_f) and the coarse mode (Cv_c), and the ratio (Cv_c/Cv_f) at Dunhuang

Date	8 Apr.	9 Apr.	26 Apr.	27 Apr.	28 Apr.	Ave.[1]	Ave.[2]
Cv_f	0.03	0.037	0.048	0.038	0.051	0.041 ± 0.01	0.044 ± 0.01
Cv_c	0.44	0.49	0.77	0.7	0.64	0.61 ± 0.14	0.65 ± 0.12
Cv_c/Cv_f	14.8	13.2	16	18.3	12.6	14.9 ± 2.3	15.0 ± 2.6

[1]Averaged for all data [2]Averaged except 8 Apr. data

Table 5. Parameters for cases 1 and 2 for group 6 at Osaka, linear particle depolarization ratio (δ_p^S) at 440, 675, 870, and 1020 nm derived from the Sun/sky radiometer data, absorption-related Ångström exponent ($å_A$), ratio of the volume concentration (Cv_c/Cv_f), coarse-mode fraction on the basis of the volume concentration (CMF_{vc}), and dust ratio (R_D) at 1020 nm.

	δ_p^S				$å_A$	Cv_c/Cv_f	CMF_{vc}	R_D
	440 nm	675 nm	870 nm	1020 nm				
Case 1	0.19 ± 0.02	0.24 ± 0.01	0.27 ± 0.01	0.29 ± 0.01	2.12 ± 0.38	6.8 ± 0.7	0.87 ± 0.01	0.88 ± 0.02
Case 2	0.15 ± 0.02	0.24 ± 0.01	0.26 ± 0.01	0.27 ± 0.01	1.58 ± 0.09	11.8 ± 1.8	0.92 ± 0.01	0.81 ± 0.03

Figure 1

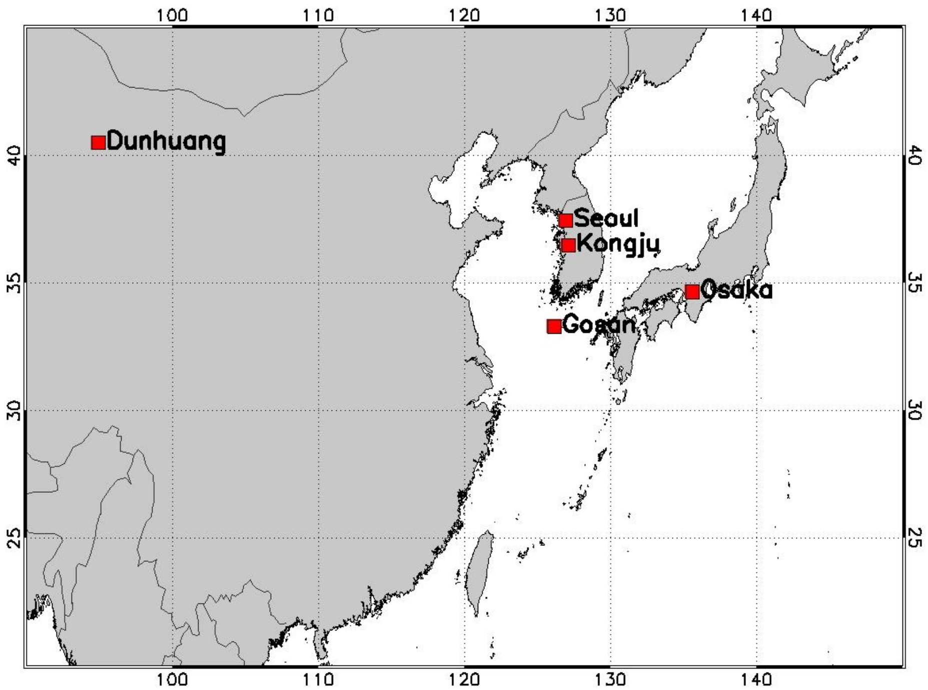
100
110
120
130
140
40
35
30
25
Dunhuang
Seoul
Kongju
Gosan
Osaka

Figure 2

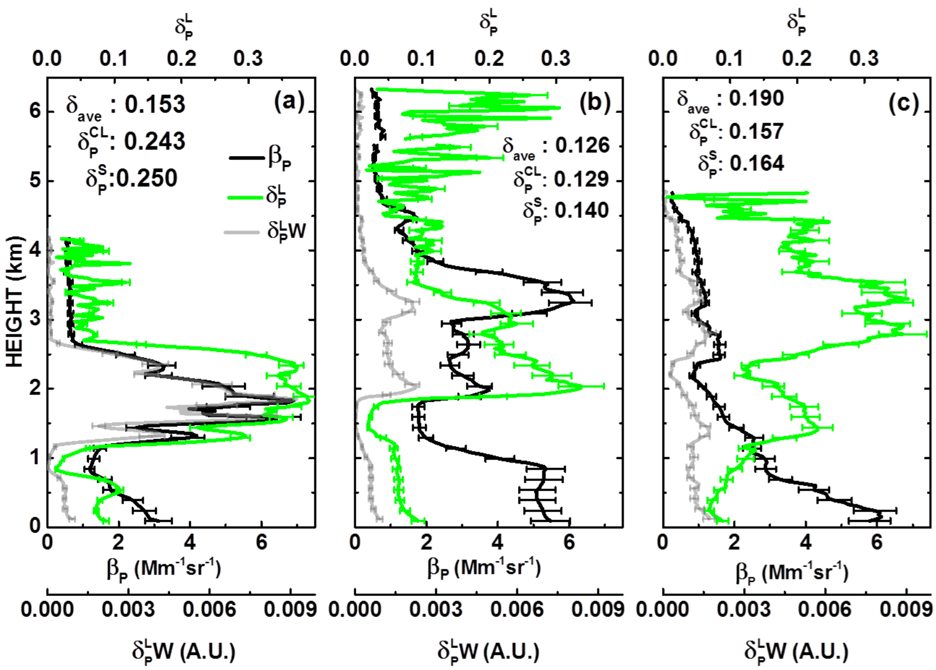
(a)
δave : 0.153
δPCL: 0.243
δPS:0.250
βP
δPL
δPLW
HEIGHT (km)
βP (Mm-1sr-1)
δPLW (A.U.)
(b)
δave : 0.126
δPCL: 0.129
δPS: 0.140
(c)
δave : 0.190
δPCL: 0.157
δPS: 0.164

Atmos. Chem. Phys. Discuss., doi:10.5194/acp-2016-1181, 2017
Manuscript under review for journal Atmos. Chem. Phys.
Discussion started: 17 February 2017

Atmospheric Chemistry and Physics
Discussions

Figure 3

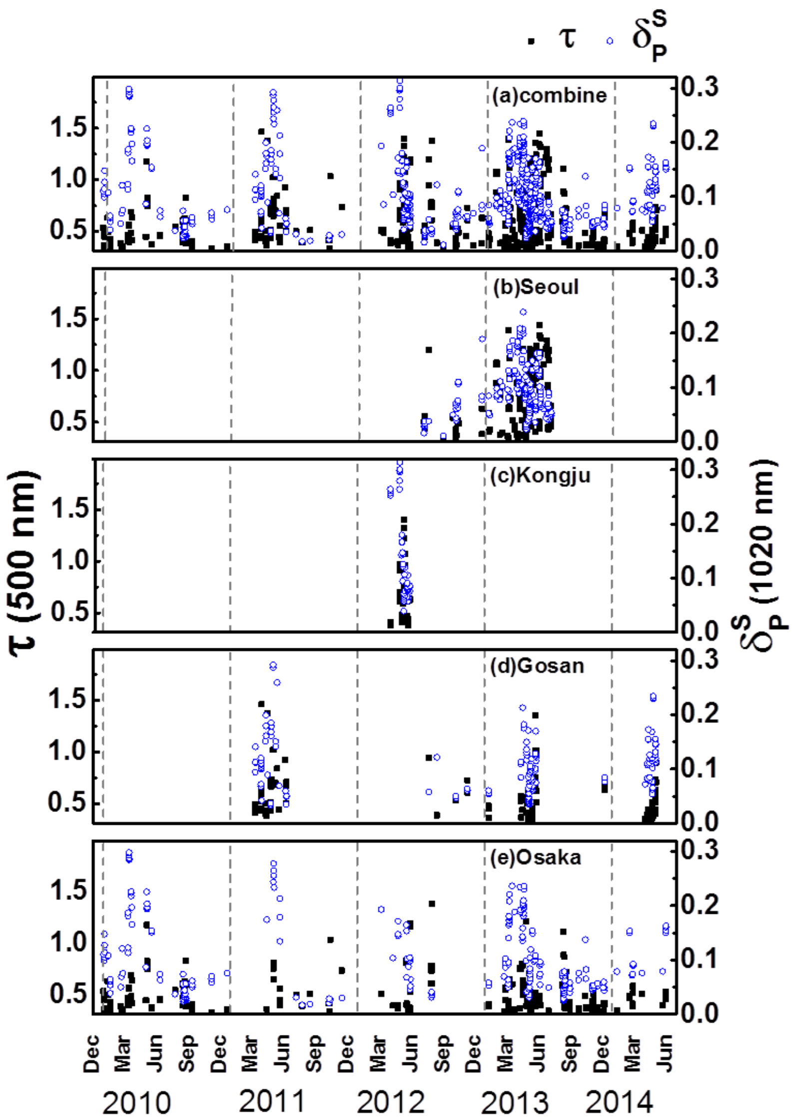

Atmospheric Chemistry and Physics Discussions
Open Access
EGU

Figure 4

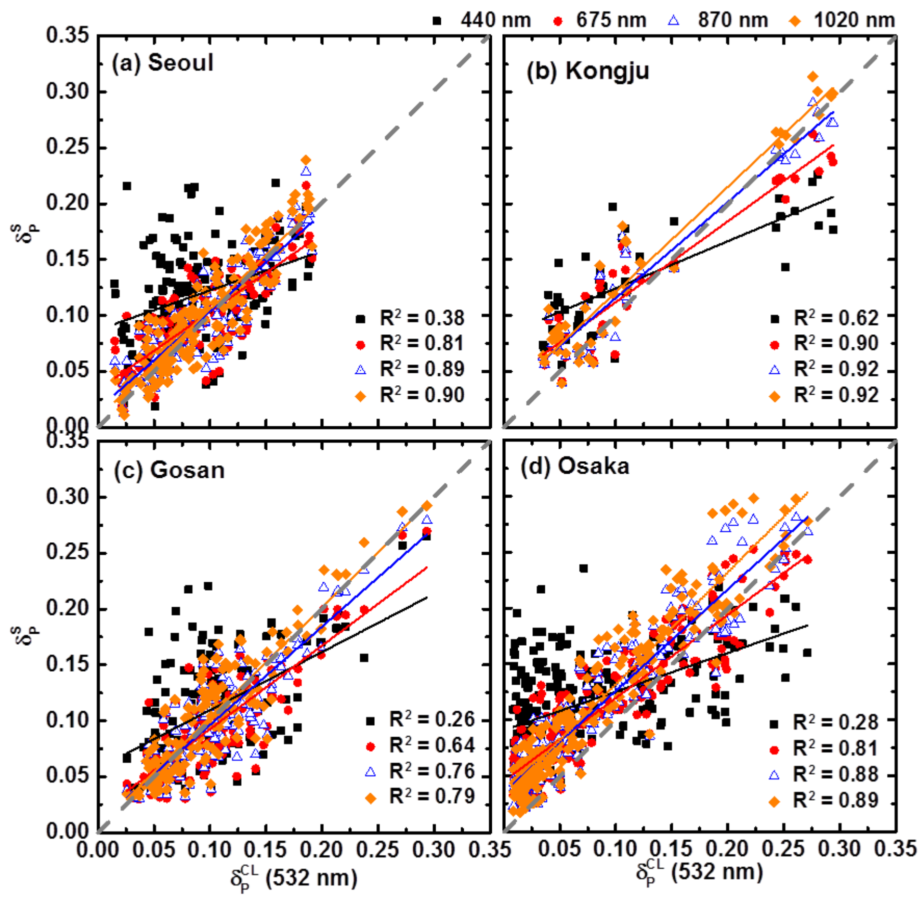

Atmos. Chem. Phys. Discuss., doi:10.5194/acp-2016-1181, 2017
Manuscript under review for journal Atmos. Chem. Phys.
Discussion started: 17 February 2017

Atmospheric Chemistry and Physics Discussions
Open Access

Figure 5

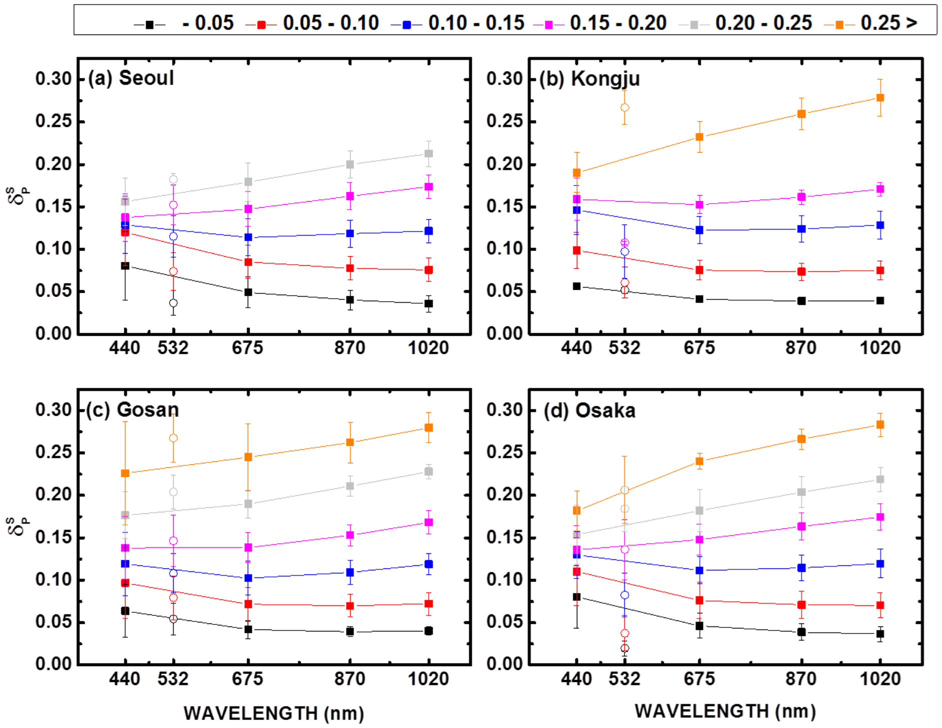

Atmos. Chem. Phys. Discuss., doi:10.5194/acp-2016-1181, 2017
Manuscript under review for journal Atmos. Chem. Phys.
Discussion started: 17 February 2017

Figure 6

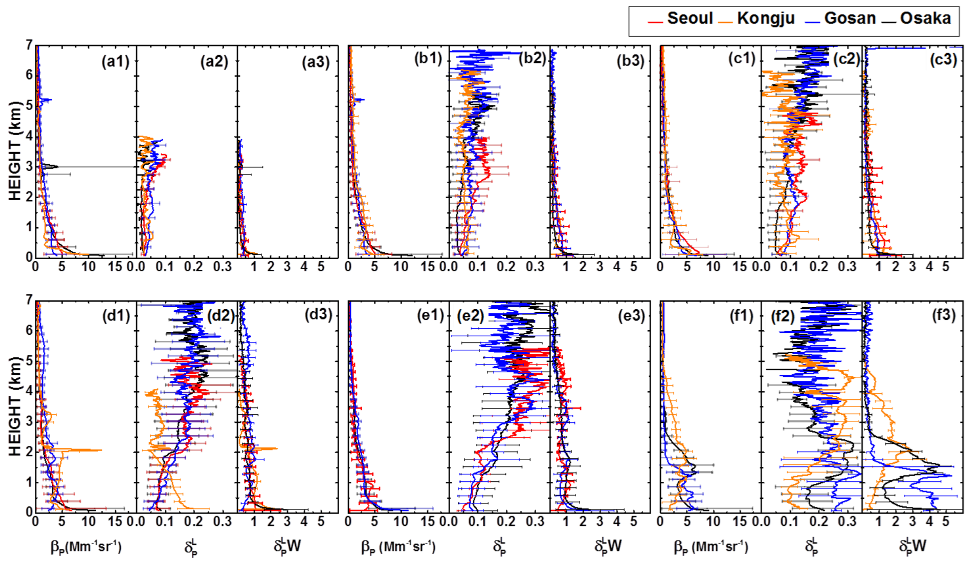

Atmos. Chem. Phys. Discuss., doi:10.5194/acp-2016-1181, 2017
Manuscript under review for journal Atmos. Chem. Phys.
Discussion started: 17 February 2017

Atmospheric Chemistry and Physics
Discussions

1061 Figure 7

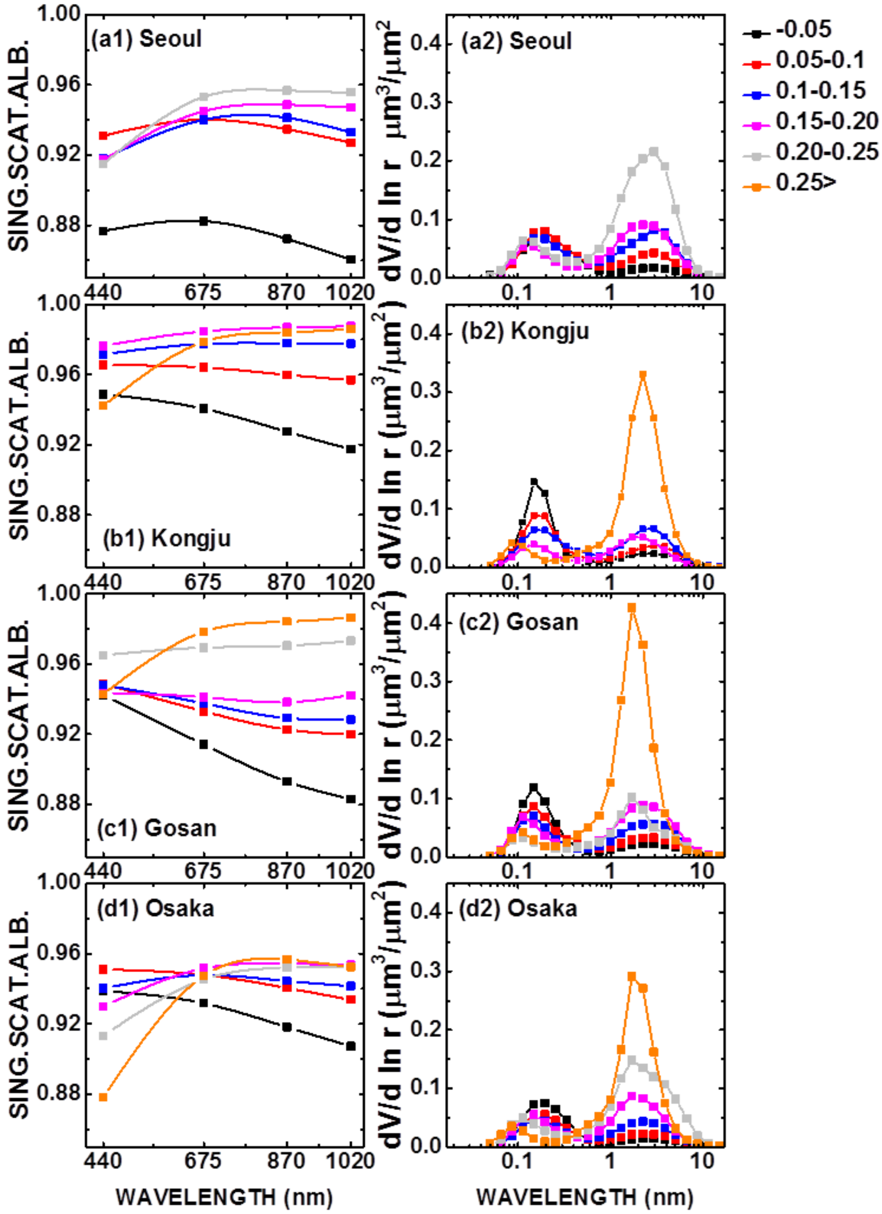

1062

Atmos. Chem. Phys. Discuss., doi:10.5194/acp-2016-1181, 2017
Manuscript under review for journal Atmos. Chem. Phys.
Discussion started: 17 February 2017

Figure 8

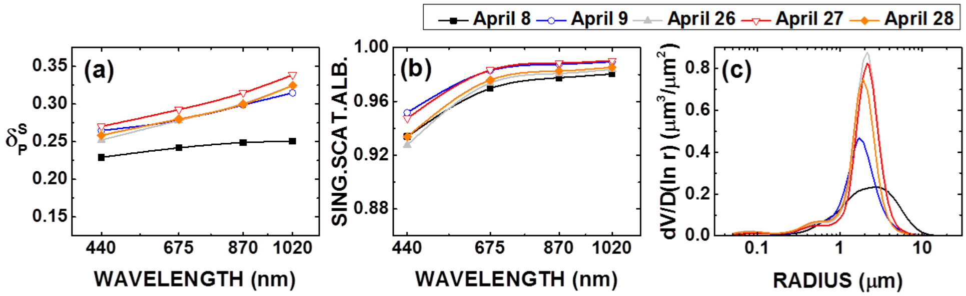

Figure 9

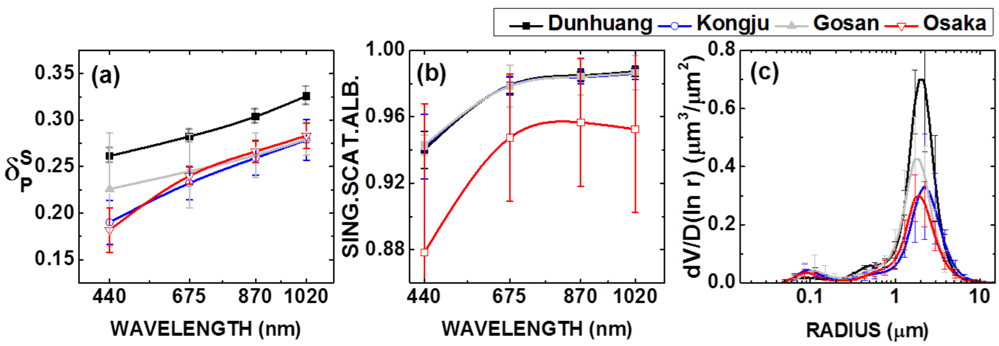

Atmos. Chem. Phys. Discuss., doi:10.5194/acp-2016-1181, 2017
Manuscript under review for journal Atmos. Chem. Phys.
Discussion started: 17 February 2017

Figure 10

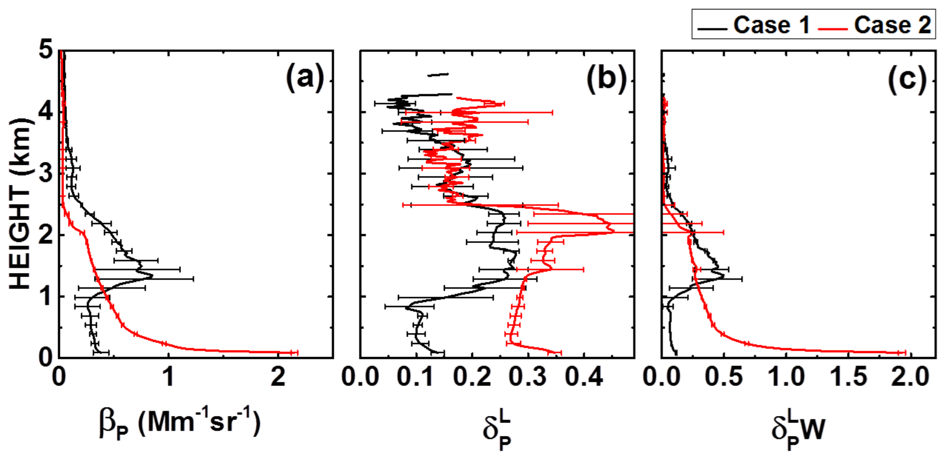

Figure 11

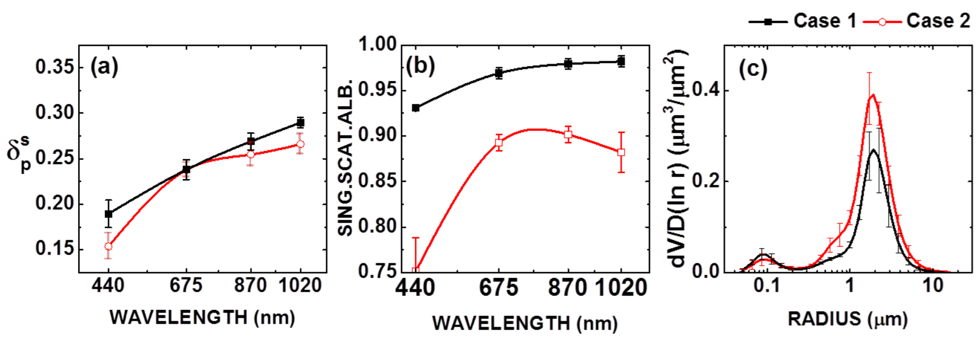

Atmos. Chem. Phys. Discuss., doi:10.5194/acp-2016-1181, 2017
Manuscript under review for journal Atmos. Chem. Phys.
Discussion started: 17 February 2017

Figure 12

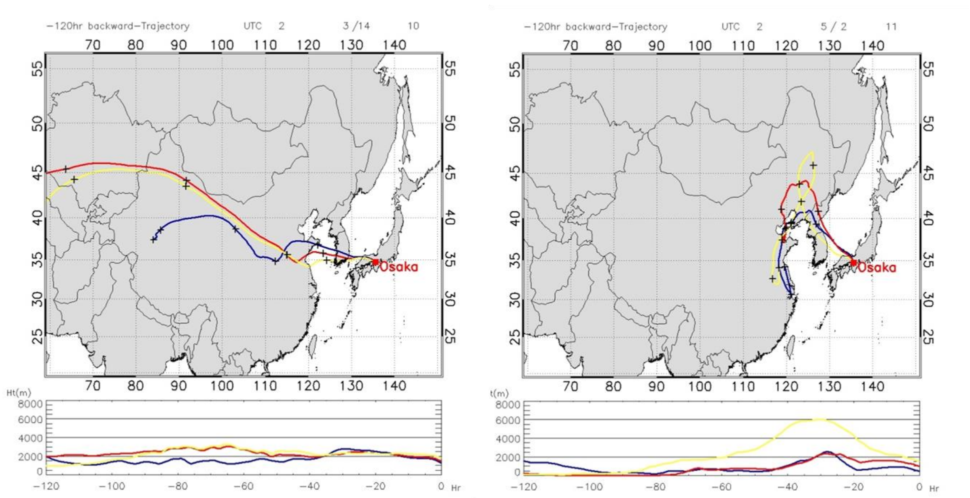

1102 Figure 13

1103